

acp-2014-267

Referee #1 comments

Author's reply shown in indented italics

A draft of the revised manuscript is appended to this document.

General Comments

The manuscript presents results from field measurements obtained from two structurally different terrain: Big Southern Butte which is about 800 m tall, and a steep river canyon in Idaho. I commend the authors for undertaking this work as there is a need for observational data for complex terrain wind models. These two cases significantly differ from existing complex terrain studies. Based on their observations, authors also make a valid point regarding the use of numerical weather models with insufficient resolution for complex terrain regions. The manuscript is written clearly and data is presented in a way that can be used for model evaluation. Therefore, I am in favor of its publication in this journal after the authors address the following issues in a revised version.

--The authors thank this reviewer for the positive and encouraging comment. Of course we feel the same and are excited to get this data out for use by others.

Specific Comments

1) Line 5 on page 16823: mention wind forecasting and resource assessment in addition to wind turbine siting.

--These additional examples have been added to this sentence. See line 52 and 53 of draft manuscript attached below.

2) Line 15 on page 16824: Askervein Hill study should be cited and mentioned.

--The Taylor and Teunissen study referenced here is the Askervein Hill study; however, we have explicitly included the name "Askervein Hill study" in this sentence as well. See line 96 of draft manuscript.

3) Although the information is available in the main text, figure captions should convey more information.

--Figure captions have been modified to ensure they are stand-alone. For example, BSB and SRC will be spelled out as Big Southern Butte and Salmon River Canyon, the time zone has been added where appropriate.

4) Provide a table for measurement coordinates. Abbreviations for sensor locations need to be spelled out in a table (R, TSW, etc.) It gets confusing after a while.

--This type of table was not originally included in an attempt to reduce the length of the manuscript (the table will be large due to the large number of sensor locations, 53 at BSB and 27 at SRC); This information is available in the database referenced in the manuscript and all sensor locations are shown on the map in Figure 1 which we will enlarge for the final published version. At this point we choose not to include it. However, if the editor recommends we can include such a table.

5) Some of the figures are too small in the printer friendly version of the manuscript. Fig 1b-d, Figs 4,6,7,8,9, 10, 12

--We have attempted to enlarge the figures to ensure they are readable in the printer-friendly version.

6) Authors collected wind profiles upstream of the BSB. Those vertical profiles should be presented and discussed for each of the regimes in light of theoretically expected profiles.

--Yes, the near-surface wind observations were part of a larger field campaign in which radar profiler, sodar, sonic anemometer, and radiosonde measurements were also made for selected time periods. It is beyond the scope of this paper, however, to present all data collected from the various instruments operated during the larger field campaign. The goals of this paper are to (1) give an overview of the measurements made during the larger field campaign (as an introduction to the field campaign – this is the first paper resulting from the study), (2) describe how others can access these data, and (3) to present the near-surface wind fields measured over the terrain obstacles at each site in order to investigate the spatial effects of the terrain on the flow. These goals are stated in lines 7-15 on p. 16825. We chose to focus on the surface wind measurements in this paper because the very high spatial resolution of the surface wind measurements made during these field campaigns is

perhaps the most unique contribution of this work, as essentially no datasets exist in the literature with this high of sensor resolution on a terrain feature of this size. These high-resolution wind data are crucial for developing and evaluating high-resolution wind models. The vertical profile data are available in the database as described in the text.

7) Provide information on the limitations of the instrumentation (e.g. threshold speeds)

--Yes, details on instrument limitations have been added in the text. For example additional discussion to the following effect has been in section 3. The cup and vane has a measurement range of 0 to 44 m/s, accuracy of ± 0.5 m/s and ± 5 degrees with resolution of 0.19 m/s and 1.4 degrees.

The Campbell Scientific CSAT3 sonic anemometers have a measurement rate of 1 to 60 Hz, with resolution of 1mm/s, 0.5 mm/s and 15mm/s for u_y , u_z and c respectively, with a direction resolution of 0.06 degrees rms. The SATI/3Vx has measurement range of 0 to 20 m/s, with resolution of 10 mm/s and 0.1 degrees.

The Scintech MFAS samples velocities from 0 to 50 m/s up to 1000 m agl over 1 to 60 min averaging intervals, with horizontal wind speed uncertainty of 0.3 m/s and vertical wind speed accuracy of 0.1 m/s and directional uncertainty less than 1.5 degrees.

The Imet-1 system has a maximum range of 250 km to altitude of 30 km and measures air pressure, temperature, and humidity. Wind speed is calculated from onboard GPS measurements. Accuracy is 0.5 hPa in pressure, 0.2 C in temperature, and 5% in RH. Wind speed is accurate to within 1 m/s and is updated at 1 Hz. Altitude is accurate to within 15 m.

The Vaisala WXT520 measures air temperature to 60C with ± 0.3 C accuracy and 0.1C resolution, Wind speed is measured from 0 to 60 m/s with 0.25 s response time and $\pm 3\%$ accuracy in speed and 0.1 degree accuracy in direction.

8) As the authors state in the Instrumentation section, they have collected data to quantify turbulence, friction velocity, sensible heat flux, temperature and relative humidity. These quantities need to be presented, and discussed in a way that can help modelers.

--We appreciate this recommendation. However, as outlined in #6 above, presenting all data from all instruments is beyond the scope of the paper and would render the paper much too long. Specific quantities like these can easily be computed from the data.

9) Figure 3. I understand that the threshold was chosen after a visual inspection. However authors can still provide a percentile for this threshold (What percentage of data is below this value?)

--Yes, we added the following statement "83% and 80% of the data fell below these threshold speeds at BSB and SRC, respectively." .

Referee #2 comments

Author's reply shown in indented italics

General comments:

The authors give an overview of two very unique new datasets collected in two types of complex terrain. In two separate summer field campaigns, near-surface wind data at 3.3 m agl at 50+ locations was collected (1) on and around an isolated mountain (Big Southern Butte, 800 m relief) and (2) in the 550-m deep Salmon River Canyon.

The methodology of binning the dataset in synoptically forced and thermally driven regimes based on a threshold wind speed at one single site has caveats that become obvious from the results but are not thoroughly discussed. These problems lead to exceptions from the expected results (such as 'downslope winds' of 12 m/s on top of BSB; even the 7.5 m/s wind speeds are doubtful (Fig5b)) that are then discussed and excluded. See more details in specific comments below. The failure of this method casts doubt on the presented results. Maybe a case study approach would be more useful and could better test and improve the current concepts of thermally driven flows in complex terrain.

--We respectfully disagree with the reviewer on the point that binning of the datasets into synoptically forced and thermally forced regimes led to exceptions which render the analysis unpublishable. Synoptic effects and local thermal effects are always combined to some extent; the goal of the partitioning scheme was to separate these effects to the best extent possible in order to focus on the predominant driving mechanism at a given time period. Had this type of binning not been used, we would not have been able to identify the average flow characteristics during the monitoring period (months of observations at each site). The goal was not to evaluate only one or two specific events, but to provide a description of the general flows over the study period – in our opinion this could only be done by using some type of data partitioning and averaging schemes.

We believe that the methods used revealed interesting characteristics of the flow at the two sites. For example, analysis at Big Southern Butte showed that under periods when most locations on the butte were experiencing diurnal flows, ridgetop locations were experiencing higher wind speeds, suggesting that ridgetop locations were decoupled from other locations on and around the butte. These types of findings have important implications for surface wind flow modeling.

We argue that the approach we used is a logical one since strong wind events overpower the local thermal effects which dominate during the diurnal flow regime.

168 *There were obviously times when synoptically-forced flows occurred and times when*
169 *diurnal flows dominated. The goal of partitioning the data was to bin the data into*
170 *discrete periods during which the flow was predominantly driven by a common force*
171 *(i.e. synoptic or local thermal effects). Of course due to the topographical complexity*
172 *of both sites as well as the shear magnitude of the geography it would seem unrealistic*
173 *to expect any single partitioning scheme would fully resolve the flows at all locations.*
174 *Thus we maintain that the partitioning scheme used is a reasonable attempt to bin the*
175 *data into interpretable chunks appropriate for the purposes and scope of this study.*

176
177
178 Other than comparing trends of down- and upslope flows with distance up and down
179 topography gradients, however, the article does not provide any significant scientific
180 results. The goal of this article remains somewhat unclear, other than reporting on a
181 new dataset.

182
183 *--We regret that the reviewer did not capture the objective of this manuscript. We*
184 *attempted to clearly state in lines 17-23 of page 16823 that the objective was to*
185 *describe a research program and associated datasets from two different terrain*
186 *features. We also stated that the intent was to provide these high resolution data to*
187 *the larger meteorological modeling community for comparison against simulations. It*
188 *is our intent that these data inform the development of high resolution near surface*
189 *wind flow models.*

190
191 The authors have a unique new dataset to analyze which mirrors the complex
192 interplay of thermally driven flows on different scales. The rather crude approach,
193 however, leads to a confusing picture and no clear results. This analysis, in my
194 opinion, needs more work is not publishable in its present form.

195
196 *--Clearly, the reviewer agrees that the data are unique in that they characterize*
197 *thermally and mechanically driven flow at a very high spatial resolution. Part of the*
198 *difficulty in evaluating a dataset like this is that the flow is driven by a complex*
199 *interplay between thermal and synoptic processes that are varying in time and space.*
200 *Thus our "crude" attempt at differentiating the data into different flow regimes. As*
201 *stated above the primary objective was to present the data in a quantitative format to*
202 *give an overview of the surface flow characteristics. Thus the logic for the "binning"*
203 *methods. We argue that the primary point is not the partitioning method, but rather*
204 *the high resolution data themselves. We leave it to future users of the data to select*
205 *whatever partitioning schema seems best for their particular needs. The point of the*
206 *analysis was not to investigate specifically upslope or downslope winds, but rather to*
207 *assess the actual surface observations under the range of flow regimes experienced at*
208 *these sites under summer meteorological conditions.*

209
210 Specific comments:

1) Thermally driven flows in complex topography are a key topic in mountain meteorology. The manuscript lacks references to some relevant articles and reviews such as Defant (1949), Whiteman (2000) and Zardi and Whiteman (2013).

--We appreciate this suggestion and have included these additional references in the section referencing other work, for example modifying lines 25 to 30 on page 16824 to read "Fine-scale (i.e., ~1-100 m) variations in topography and vegetation substantially alter the near-surface flow field through mechanical effects, such as flow separation around obstacles, enhanced turbulence from increased surface roughness and speed-up over ridges, and through thermally-driven flows induced by local differential surface heating in steep terrain (Defant, 1949; Banta, 1984; Banta and Cotton 1982; Whiteman, 2000; Zardi and Whiteman, 2013; Chrust, et al., 2013). "

2) "Upvalley drainage winds" are listed as a mechanism to couple the surface flow to the synoptic flow. Drainage winds are usually related to the fact that denser air drains down a topographic gradient. It is not clear what process the authors are referring to.

-- The referee has not provided sufficient context for us to clearly determine where his/her concern lies. Therefore, a specific response to this comment is difficult because it is not clear to which line/page the reviewer is referring.

3) A paragraph describing the surface flow field that is expected in the current state of knowledge at each the two study sites under the 'diurnal wind regime' could be included to set the stage for the findings.

--Thank you for this comment. We direct the reviewer to lines 7-12 on page 16826 and lines 2-10 of page 16827 for this information. We have also added further discussion of diurnal flow at the beginning of sections 5.1.1 and 5.2.1. .

4) Binning into synoptically forced regime: The authors chose to use one single representative site for each experiment for which threshold wind speeds are determined that will separate thermally driven and synoptically driven regimes. What are the caveats of this methodology? For example, a "reference station" on the plain surrounding BSB was chosen (R2) to distinguish between the two regimes. How likely is it that this station will be dominated by nocturnal thermally driven flows in the evening while the flow on the butte is not? On the other hand, NM1 was chosen as "reference station" for the Salmon River Canyon site, which is ~500 m (?) above the canyon bottom. How likely are thermally driven flows still dominating the river gorge when a synoptic influence is seen at the reference site? A thorough discussion of the implications of this filtering method is needed. Furthermore, the methodology seems to fail, and while extreme events such as drainage flows on top of BSB of 12 m/s are discussed as outliers, speeds of 7.3 m/s are reported as valid data points (Fig 4b).

-- The overall goal was to present the average flow fields at each site in a context useful for surface wind flow modeling applications. We chose to present average flows for the four wind regimes described in section 4.1. The regimes listed in 4.1 are widely recognized in the mountain meteorology literature (e.g., Banta and Cotton, 1982; Whiteman, 2000). In order to summarize months of wind data at each site in terms of these flow regimes, we had to choose a partitioning scheme to bin the data. Many different partitioning schemes could have been used. We believe our choice of selecting a single representative sensor at each site to partition the flow was a reasonable approach for the purpose and scope of this study.

It is possible that our selected reference station at the butte, for example, could “be dominated by nocturnal thermally driven flows in the evening while flow at some locations on the butte is not.” In fact, this is precisely the type of unique flow features we would like to uncover in this work, as this is the type of information that is lacking in the literature, but could be very useful to surface wind model developers. We explored wind data from the INL mesonet station (already described in the text) on the summit of Big Southern Butte as a potential indicator of the gradient level winds. We included discussion at the end of section 4.1 in an effort to facilitate the discussion around lines 4-16 on page 16835.. We do not report the observed ridgetop high winds (e.g., 12 m/s) during the diurnal regimes as thermally driven winds, but rather point out that these ridgetop locations appear to be decoupled from the diurnally driven flows at other locations on and around the butte. We point out that ridgetop locations appear to often be more closely coupled with the gradient level winds. Inclusion of the mesonet data from the summit of Big Southern Butte (as described above) will help to demonstrate this point. Flows described in this paper as “upslope” and “downslope” fall within the range of slope flows reported in the literature (e.g., see discussion on p 13-14).

5) BSB: The “afternoon regime” vector map (Fig 4) could be interpreted as a flow field based purely on daytime thermally driven circulations where upslope and upvalley flows interact. How is the distinction made between a purely thermally driven flow regime and a situation with a synoptic influence? R2 shows only a weak flow (maybe 4 m/s?; see comment on presentation) around the obstacle.

--This is also true and it is probably not possible to say for sure which mechanism is at play. Wind speeds would not need to be high in order for convective mixing to play a role. Prevailing gradient-level winds were often from the southwest, which is in

alignment with upvalley flow on the snake river plain in the vicinity of the butte. We describe the flows in the “afternoon regime” as developing from convective mixing of gradient-level wind into the growing boundary layer, as described by Banta and Cotton (1982). This is a reasonable explanation that is supported in other reported studies, although as pointed out, there could potentially be other mechanisms driving this “afternoon regime.” Ultimately, it is the observed surface wind field that we are interested in presenting and we clearly observed a unique “afternoon regime.” We can really only speculate on the forcings which may have set up this afternoon flow field (it is beyond the scope of this study to investigate the larger scale forcings). Convective mixing is one likely mechanism.

6) Figure 12 includes a site (NM2) that was in an earlier thorough discussion characterized as an outlier. It therefore should be omitted and not presented as part of a elevation transect.

--The term outlier is not used anywhere in the manuscript and we apologize if we implied that NM2 should be considered so. We did not intend to imply or describe NM2 as an outlier. We speculate that this sensor may have been in a zone of recirculation, but we have no reason to suspect that the data are not good therefore we cannot justify omitting the data from this sensor.

7) Standard times should be used instead of daylight savings time.

-- Our logic for presenting time as local daylight time was that it does not require the reader to do any conversions to estimate solar position at a given time. We prefer to keep the local time format.

8) What is the role of terrain shading at the SRC site? What are its implications on the timing of the transitions between thermally driven flow regimes?

--Terrain shading is a likely contributor to the local surface flows at both sites, particularly under the diurnal wind regime, however, we did not investigate it in this version of the manuscript. We recommend that it be considered in detail in a future analysis and manuscript separate from this study that is primarily focused on summarizing the data.

9) The manuscript unnecessarily describes sodar and radiosonde observations and deployment schedules. This should be omitted, as none of the data is presented or used in the presented analysis.

--One of the goals of the paper is to introduce the larger field campaigns, which included these additional measurements. We would like to describe the methods used and how to access these data, although it is beyond the scope of the paper to provide analyses of these data (the focus here is on the near-surface wind observations). As this is the first paper to stem from this larger field campaign, we feel it is appropriate to describe the full dataset here, while saving in-depth analyses of some of the data for future work.

10) Presentation:

Overall graphic presentation is fair and could be substantially improved:

a) Maps: The article lacks bigger and clearly readable maps for the two field sites. Instead of several subfigures covering different geographic extents, a full-page figure is needed with readable labels of the sites and elevation contours. A distance scale is needed; different symbols could be used for the different instrumentation. Transects later referred to could be marked and labeled.

--Where possible the overview maps have been enlarged to a full-figure page. Lat/lons of the study area are currently provided, and a distance scale has been included in all relevant images. Elevation contours are shown in the figures that depict the terrain. However, the contours are faint lines, we prefer this approach to provide more clarity to for the sensor locations and associated wind vectors. In our opinion, enhancing the elevation contours would make it more difficult to distinguish the relevant data

b) Wind vector graphics: Color bar could be extended; a reference-length vector could be included. Two bigger figures would be better than 4 small sub-figures. Key locations referred to in the text discussing these figures should be labeled. A cross reference with the initial maps is extremely tedious for the interested reader. Figures could be formatted to fill the space available on a page.

--The color bar has been moved so that it is in the figure itself. The figures have been enlarged so that two figures are used at the full extent, rather than a zoomed-in version and the full-extent version. Key locations are marked. Final formatting to fit the page/text will be handled by the journal.

c) Contour graphics: Color scales could be kept constant for all sub-figures. Otherwise a comparison is not possible.

--Yes, thank you for this observation we believe we have improved the presentation of color scales and graphics in the revision.

d) All subfigures should be labeled, i.e. Fig 4a through 4f.

--Yes, all subfigures have been labeled in the revised manuscript.

11) SRC: How could the available, but not presented, temperature data help to evaluate different regimes?

--We have temperature data for one ridgetop location and one valley bottom location for select time periods during the field campaign. We considered looking into these temperature data to determine if there is any information to add to the discussion. However, the partitioning method based solely on time of day and threshold wind speed appears to work well for binning the data into various flow regimes (as evidenced by the vector plots), thus at this point we have not explored the temperature data further. The data are available in the archived dataset.

12) Wind speed trends presented in Fig 10 are rather small. How do they compare to the uncertainty of the anemometers?

--Thank you for this observation, we have added some discussion regarding the uncertainty of the anemometers within the context of the reported trends (see section 3).

13) Correlations with gradient level winds are mentioned in the conclusions. How were gradient level winds determined for the period of observations? They should be presented earlier in the manuscript. Could they be used to filter the dataset, rather than selected surface observations?

--In the current version of the manuscript, actual measures of gradient level winds are not reported. We described some ridgetop observations as being correlated with gradient level winds when ridgetop observed speeds were much higher than other nearby observed surface speeds during the diurnal flow regime. These are qualitative statements based on the assumption that the gradient level wind speeds are likely higher than the speeds measured by our non-ridgetop surface sensors. In the revised manuscript state that we explored data from the INL mesonet station at the summit of Big Southern Butte as a measure of the gradient level wind at this site for comparison against our surface observations. We investigated the sodar and radiosonde data for gradient level winds at the Salmon River Canyon site. For time periods during which we do not have sodar or radiosonde data, we explored archived mesoscale forecast data as an estimate of the gradient level winds at this site. This proposed presentation of measured gradient level winds strengthens the discussion, especially on the topic of ridgetop wind decoupling from the rest of the surface flow.

416 Technical corrections:

417 - Decapitalize "s" in "radiosonde" (i.e. page 16829, line 3)

418

419 *--suggestion incorporated*

420

421 - p 16828 | 2 Table 2 does not list AWS

422

423 *--could not find a single reference to AWS in the manuscript, not sure what the*
424 *reviewer is referring to.*

425

426 - Reduce number of digits in GPS readings

427

428 *--Incorporated in all GPS references.*

429

430 - p 16826 | 5 ; change "down-drainage" flows to "down-valley" flows

431

432 *--Modified as suggested.*

433

434 - p 16830 | 18: could be clarified by expanding to "... into the forth, synoptically
435 forced, regime."

436

437 *--Modified as suggested*

438

439 - Fig 6: Label subfigures with site elevations. Mention filtering (Thermally driven
440 regime) at the beginning of caption.

441

442 *--Figure captions modified to state elevations of applicable sensors or general*
443 *location. Filtering also included.*

444

445 Label key directions (upvalley & downvalley, upslope and downslope) in figures.

446

447 *--In all figures referring to Big Southern Butte the topographical gradient is*
448 *increasing from south to north. In the Salmon River Canyon the gradient is*
449 *increasing elevation from left to right. We have added this statement in the site*
450 *locations.*

451

452

453

1 |

High Resolution Observations of the Near-Surface Wind Field over an Isolated Mountain and in a Steep River Canyon

B.W. Butler^{1,4}, N.S. Wagenbrenner^{1,2}, J.M. Forthofer¹, B.K. Lamb², K.S. Shannon¹, D. Finn³, R. M. Eckman³, K. Clawson³, L. Bradshaw¹, P. Sopko¹, S. Beard³, D. Jimenez¹, C. Wold¹, M., Vosburgh¹

[1]US Forest Service, Rocky Mountain Research Station, Missoula Fire Sciences Laboratory, 5775 Hwy 10 Missoula, MT 59808

[2]Washington State University, Laboratory for Atmospheric Research
Pullman, WA 99164-2910

[3]NOAA Air Resources Laboratory, Field Research Division 1750 Foote Dr.
Idaho Falls, ID 83402

[4]Corresponding Author t:406-329-4801, c:406-239-3665, f:406-329-4825,
e:bwbutler@fs.fed.us

Abstract

A number of numerical wind flow models have been developed for simulating wind flow at relatively fine spatial resolutions (e.g., ~100 m); however, there are very limited observational data available for evaluating these high resolution models. This study presents high-resolution surface wind datasets collected from an isolated mountain and a steep river canyon. The wind data are presented in terms of four flow regimes: upslope, afternoon, downslope, and a synoptically-driven regime. There were notable differences in the data collected from the two terrain types. For example, wind speeds on the isolated mountain increased with distance upslope during upslope flow, but generally decreased with distance upslope at the river canyon site during upslope flow. In a downslope flow, wind speed did not have a consistent trend with position on the isolated mountain, but generally increased with distance upslope at the river canyon site. The highest measured speeds occurred during the passage of frontal systems on the isolated mountain. Mountaintop winds were often twice as high as wind speeds measured on the surrounding plain. The highest speeds measured in the river canyon occurred during late morning hours and were from easterly downcanyon flows, presumably associated with surface pressure gradients induced by formation of a regional thermal trough to the west and high pressure to the east. Under periods of weak synoptic forcing, surface winds tended to be decoupled from large-scale flows, and under periods of strong synoptic forcing, variability in surface winds was sufficiently large due to terrain-induced mechanical effects (speed-up over ridges and decreased speeds on leeward sides of terrain obstacles) that a large-scale mean flow would not be representative of surface winds at most locations on or within the terrain feature. These findings suggest that traditional operational weather model (i.e., with numerical grid resolutions of around 4 km or larger) wind predictions are not likely to be good predictors of local near-surface

winds at sub-grid scales in complex terrain. Measurement data can be found at: <http://www.firemodels.org/index.php/windninja-introduction/windninja-publications>.

1 Introduction

Predictions of terrain-driven winds are important in regions with complex topography for a number of issues, including wildland fire behavior and spread (Sharples et al., 2012; Simpson et al., 2013), transport and dispersion of pollutants (Jiménez et al., 2006; Grell et al., 2000), simulation of convection-driven processes (Banta, 1984; Langhans et al., 2013), wind [resource assessment for applications such as wind turbine siting](#) (Chrust et al., 2013; Palma et al., 2008), [wind forecasting \(Forthofer et al., in press\)](#), and climate change impacts (Daly et al., 2010). Numerous efforts have focused on improving boundary-layer flow predictions from numerical weather prediction (NWP) models by either reducing the horizontal grid size in order to resolve the effects of finer-scale topographical features on atmospheric flow (Lundquist et al., 2010; Zhong and Fast, 2003) or adding new parameterizations to account for unresolved terrain features (Jiménez and Dudhia, 2012). Because NWP simulations are computationally demanding and suffer from inherent limitations of terrain-following coordinate systems in steep terrain (Lundquist et al., 2010), a number of high resolution diagnostic wind models have also been developed to downscale wind predictions from NWP models in order to meet the needs of the aforementioned applications (e.g., Beaucage et al., 2012). However, there are limited observational data available to evaluate and improve such high resolution models. This paper describes a research program in which wind data were collected at very high spatial resolution under a range of meteorological conditions for two different types of complex terrain features. The datasets collected enhance the archive of observational data available to evaluate high resolution models. All of the data from the field program are available at: <http://www.firemodels.org/index.php/windninja-introduction/windninja-publications>.

Fine-scale (i.e., ~1-100 m) variations in topography and vegetation substantially alter the near-surface flow field through mechanical effects, such as flow separation around obstacles, enhanced turbulence from increased surface roughness and speed-up over ridges, and through thermally-driven flows induced by local differential surface heating in steep terrain ([Defant, 1949](#), [Banta, 1984](#); [Banta and Cotton, 1982](#); [Whiteman, 2000](#), [Zardi and Whiteman, 2013](#), [Chrust, et al., 2013](#)~~[Defant, 1949](#), [Banta, 1984](#); [Banta and Cotton, 1982](#); [Whiteman, 2000](#), [Zardi and Whiteman, 2013](#), [Chrust, et al., 2013](#)~~). These local scale flow effects are critical for surface wind-sensitive processes, such as wildland fire behavior, where the near-surface wind is often the driving meteorological variable for fire rate of spread and intensity (Rothermel, 1972; Sharples et al., 2012). In order to capture these terrain-induced effects, wind modeling in complex terrain requires that surface characteristics, including terrain, vegetation, and their interactions with the atmosphere, be resolved at a high spatial resolution.

Although diagnostic wind models do not typically employ sophisticated boundary layer schemes in their flow solutions, they often incorporate parameterized algorithms for specific boundary layer effects, such as thermally-driven winds (e.g., diurnal slope flows) and non-neutral atmospheric stability (Forthofer et al., 2009; Scire et al., 2000). Evaluation of such schemes has been limited by the types of terrain features and

range of meteorological conditions represented in available observational datasets. For example, the evaluations performed by Forthofer et al. (In Review) were limited by available surface wind data in complex terrain. The two most widely used datasets for evaluation of high resolution wind predictions were collected on topographically-simple, low elevation hills investigated for wind energy applications [such as the site for the Askervein Hill study](#) (Berg et al., 2011; Taylor and Teunissen, 1987). Wind energy research has focused on relatively simple terrain because winds in complicated terrain are more difficult to reliably forecast and have higher turbulence that reduces the life of the turbines. These studies of idealized field sites have produced useful data for investigating the effects of simple terrain obstructions on average atmospheric flow and identifying specific deficiencies in numerical flow solutions; however, such sites are not representative of the wide range of regions where terrain-induced winds occur. As a result, these data do not provide sufficient test data for evaluating spatial representation of modeled flows for commonly occurring types of terrain features, such as isolated terrain obstacles with complex geometries, dissected montane environments, and steep river canyons. Other types of observational studies, such as those designed to investigate boundary layer evolution or convection-driven processes, have focused on characterizing the vertical distribution of wind, temperature, and moisture, but do not typically characterize the spatial variability in the near-surface wind field. Examples of the types of flow phenomenon that are of interest for high resolution model evaluations include 1) local surface layer flow decoupling from larger-scale atmospheric flow, 2) diurnal slope flows; 3) mountain-valley flows; 4) mountain-plain flows; and 4) the interactions of these effects at multiple spatial and temporal scales.

This study consisted of a field campaign focused on the collection of high resolution wind data from two different types of terrain features. Here we provide an overview of the data, with particular emphasis on the spatial characteristics of the surface wind measurements, and describe some unique flow features at each site.

The following presents: 1) a description of two study sites exhibiting different types of complex terrain features; 2) methods followed to collect detailed high resolution wind data over a range of meteorological conditions at each site; 3) an overview of the local meteorology and predominant flow field at each site; 4) unique surface flow features measured at each site; and 5) a description of how to access to the datasets. The data collected during this field campaign are used in a companion paper (Wagenbrenner et al., in Preparation) to evaluate several different NWP models and downscaling methods.

2 Site Descriptions

2.1 Big Southern Butte (BSB)

BSB is a volcanic dome cinder cone approximately 4 km wide that rises 800 m above the Upper Snake River Plain (USRP) in southeastern Idaho (43.3959⁵⁸, -113.0225⁷) (Fig. 1). The dominant vegetation on the USRP and BSB is grass and sagebrush (generally < 1 m tall), although a few north-facing slopes on the butte have some isolated stands of 3-10 m tall timber. Average slopes range from 30 to 40% with nearly vertical cliffs in some locations. The USRP is essentially flat terrain surrounding BSB and extends more than 120 km to the north, east, south, and southwest (Fig. 2). The USRP is bordered by tall mountain ranges to the northwest

and southeast. There are three prominent drainages (Big Lost River, Little Lost River, and Birch Creek) that flow southeast onto the USRP to the north of BSB (Fig. 2). These mountain-valley features contribute to thermally-driven diurnal flows and formation of convergence zones on the USRP. Nighttime down-drainage-valley flows on the USRP are from the northeast and daytime up-drainage flows are from the southwest.

Typical summertime winds on the Snake River Plain are primarily thermally driven with strong upvalley winds during the day and relatively weaker downvalley winds at night. The regional nocturnal northeasterly drainage flows usually subside by late morning, and winds begin to rotate clockwise to southwesterly flow, then speeds increase sharply by mid-to-late afternoon. The strongest southwesterly wind events in the summer are associated with the passage of frontal systems.

Additionally, this region experiences occasional passage of very strong frontal systems which bring westerly winds that become channeled into southwesterly flow up the Lower Snake River Plain (LSRP) toward BSB (e.g, Andretta, 2002). This same westerly synoptic flow passes over the mountains to the north of BSB and surface winds become channeled into northerly flow down the Big Lost, Little Lost, and Birch Creek drainages and onto the USRP. This northerly flow approaches BSB from the USRP, eventually converging with the southwesterly flow somewhere in the vicinity of BSB in what is referred to as the Snake River Plain Convergent Zone (SPCZ) (Andretta, 2002; Andretta and Hazen, 1998). When an SPCZ forms, its location shifts up or down the SRP depending on the strength of the low-level winds over the USRP versus the LSRP (Andretta, 2002). SPCZ events most commonly occur during the winter and spring, but occasionally form during other time periods as well. Although formation of the SPCZ is not a frequent phenomenon during summer conditions, we did observe a few flow events that may have been associated with the SPCZ during our field campaign. Because the strong frontal systems which lead to formation of the SPCZ result in complicated near-surface flows on and around BSB, we investigate the observed flow events possibly associated with SPCZ-like conditions in detail in Section 5.1.2.

2.2 Salmon River Canyon (SRC)

The field site was a 5 km long stretch of river located approximately 20 km east (upstream) of Riggins, ID (45.401667, -116.22667) (Fig. 34) and spanning in elevation from the canyon bottom (550 m) to the ridgetops (1600 m). The river canyon follows a nearly straight east-west path within this extent. Prevailing winds in this region are from the west. The predominant vegetation is grass (generally < 0.5 m tall), with some timber in the higher elevations on the north aspects. Our instrumentation was deployed away from forested areas, so as to avoid effects of the forest canopy on the wind flow. There were prominent side drainages entering SRC on the east and west end of our study area (Fig. 34).

3 Instrumentation

Each field site was instrumented with a network of surface wind sensors deployed over a several month period (hereafter referred to as the monitoring period) and supplemented with short term deployment of sonic anemometers and ground-based vertical profiling instruments. Spatially dense arrays of more than 50 cup-and-vane anemometers (S-WCA-M003, Onset Computer Corporation) measured wind speeds

and directions at 3.3 m above ground level (AGL) to characterize surface flow patterns over and within the terrain features. Wind speed and direction data were measured at 1 Hz and 30-second average wind speeds, peak gusts, and average directions were recorded. The cup and vane has a measurement range of 0 to 44 m s⁻¹, accuracy of +/- 0.5 m s⁻¹ and +/- 5 degrees with resolution of 0.19 m s⁻¹ and 1.4 degrees. These surface measurements were complemented by sonic anemometers (CSAT3, Campbell Scientific, Inc.; SATI/3Vx, Applied Technologies, Inc.) and vertical profiling instruments (MFAS, Scitech) at select locations and times (Table 1; Fig. 1 and 3) in order to provide measures of turbulence, friction velocity, and sensible heat flux in near surface flows as well as to characterize flows aloft. The Campbell Scientific CSAT3 sonic anemometers have a measurement rate of 1 to 60 hz, with resolution of 1 mm s⁻¹, 0.5 mm s⁻¹ and 15 mm s⁻¹ for ux and uy, uz, and c respectively, with a direction resolution of 0.06 degrees rms. The SATI/3Vx has measurement range of 0 to 20 m s⁻¹, with resolution of 10 mm s⁻¹ and 0.1 degrees. The Scitech MFAS samples velocities from 0 to 50 m s⁻¹ up to 1000 m agl over 1 to 60 min averaging intervals, with horizontal wind speed uncertainty of 0.3 m s⁻¹ and vertical wind speed accuracy of 0.1 m s⁻¹ and directional uncertainty less than 1.5 degrees. Radiosonde (iMet-1, International Met Systems) launches were conducted to characterize large-scale flows aloft for select time periods at each site. The Imet-1 system has a maximum range of 250 km to an altitude of 30 km and measures air pressure, temperature, and humidity. Wind speed is calculated from onboard GPS measurements. Accuracy is 0.5 hPa in pressure, 0.2°C in temperature, and 5 % in RH. Wind speed is accurate to within 1 m s⁻¹ and is updated at 1 Hz. Altitude is accurate to within 15 m. Weather stations (WXT520, Vaisala) measured relative humidity, air temperature, wind speed and direction, solar radiation, and precipitation 2 m AGL at two locations (Table 2; Fig 1 and 3). The Vaisala WXT520 measures air temperature to 60C with +/-0.3°C accuracy and 0.1C resolution, Wind speed is measured from 0 to 60 m s⁻¹ with 0.25 s response time and +/-3% accuracy in speed and 0.1 degree accuracy in direction.

The sampling layouts were designed to obtain measures of the upwind approach flows as well as perturbations to the approach flow associated with the terrain features. For each site, the extent of the sensor array covered an area that spanned one to several mesoscale weather forecast grids of typical routine forecast resolution (4 to 12 km) and the spatial density of the surface sensors was fine enough to resolve flow patterns at the sub-grid scale (Fig. 1). Two field sites were selected to represent an isolated terrain obstacle and a steep, non-forested river canyon. These sites provided a range of wind conditions representative of generally dry, inland, montane locations during summertime periods.

An array of 53 surface sensors was deployed on BSB between 15 June 2010 to 9 September 2010 (Fig. 1). Sensors were deployed along two transects running southwest to northeast. A number of randomly located sensors were added along and outside the two transects to increase the spatial coverage on and around the ~~butte~~BSB. A sodar profiler was deployed 2 km southwest of the butte from 1 July to 18 July, 2010 and immediately northeast of the butte from 31 August to 1 September, 2010 (Fig. 1; Table 1). A tower of sonic anemometers was deployed 2 km southwest of the butte from 14 July to 18 July, 2010 (Fig. 1; Table 1). Three ~~RadioSonde~~ Radiosonde launches were conducted at BSB from 31 August to 2 September, 2010 (Table 2).

An array of 27 surface sensors was deployed in three cross-river transects at SRC from 14 July to 13 September, 2011 (Fig. 34). Sodars and sonic anemometers were operated from 16 July to 18 July and 29 August to 31 August, 2011 (Table 1). Sodars were located in the valley bottom on the north side of the river and at the ridgetop on the north side of the river near the east end of the field site (Fig. 34). Sonics were operated on north and south ridgetops near the west end of the study area and at two locations in the valley bottom on the north side of the river (Fig. 1). Two weather stations monitored air temperature, relative humidity, precipitation, solar radiation, wind speed, and wind direction; one was located on the southern ridgetop at the east end of the field site and the other was located in the valley bottom on the north side of the river (Fig. 34). Six RadioSonde launches were conducted on 18 August, 2011 (Table 2).

Additionally, the National Oceanic and Atmospheric Administration Field Research Division (NOAA-FRD) operates a permanent mesonet system that consists of 35 towers spread across the Idaho National Laboratory (INL) located on the USRP and encompassing the BSB study area (<http://www.noaa.inel.gov/capabilities/mesonet/mesonet.htm>; <http://niwc.noaa.inel.gov/>). The mesonet towers measure wind speed, wind direction, air temperature, relative humidity, and solar radiation. NOAA-FRD operates a permanent wind profiling system (915 MHz radar profiler) and radio acoustic sounding system (RASS) at a location approximately 10 km northeast of BSB. NOAA-FRD also operated a mobile Radian Model 600PA SoDAR approximately 5 km south of BSB and an Atmospheric Systems Corp. (ASC) Model 4000 mini SoDAR 15 km south of BSB 15 July to 18 July, 2010 and 31 August to 2 September, 2010.

4 Analysis Methods and Terminology

The data analyses presented here focus on the surface wind measurements and terrain influences on the surface flow characteristics determined from these measurements. All data are available in public archives as described in section 5.3. All times presented are local daylight time to provide perspective on diurnal flow regimes.

4.1 Partitioning surface data into flow regimes

The surface wind data are partitioned into four distinct wind regimes in order to facilitate the analysis of typical diurnal flows in the absence of strong synoptic forcing and high wind events during periods of strong synoptic forcing. The four wind regimes are:

(1) Aa downslope regime, which included downslope and downvalley flows, forced by nighttime surface cooling under weak synoptic forcing.

(2) aAn upslope regime, which included upslope and upvalley flows, forced by daytime surface heating under weak synoptic forcing.

(3) Aan afternoon regime, during which local flows were influenced by larger scale flows, either through convective mixing (at BSB) or through formation of upvalley drainage winds (at SRC) under weak synoptic forcing.

(4) aA synoptically forced regime, during which the normal diurnal cycle was disrupted by strong larger scale flows typically correlated with gradient level winds due to mechanically-induced turbulent mixing in the boundary layer.

The first three are analogous to the wind regimes described in Banta and Cotton (1982) and are referred to collectively in this paper as the diurnal wind regime. The diurnal wind regime persisted during periods of weak synoptic forcing. The fourth regime was included here as the field sites investigated in this study frequently experienced periods of intense large-scale synoptic forcing which generated high surface wind speeds and sufficient mechanical mixing to overcome the diurnal flow regime.

The following procedure was used to partition the surface data into these flow regimes. First, periods during which the wind speed exceeded a threshold wind speed at a surface sensor chosen to be representative of the large-scale flow at each site were partitioned into a fourth, synoptically forced, regime (4). Threshold wind speeds were selected for each site based on visual inspection of the wind speed time series data for the chosen sensors. Thresholds were selected to be speeds that were just-slightly above the typical daily peak speed for the chosen sensors. In other words, the threshold speed was only exceeded when synoptic forcing disrupted the typical diurnal wind regime at a given site. Speeds below the threshold are indicative of periods of weak synoptic forcing, during which the diurnal wind regime prevails. Sensors R2 and NM1 were chosen to be the representative sensors at BSB and SRC, respectively. R2 was located on the USRP approximately 5 km southwest of the butte at 1570 m elevation. NM1 was located on the north side of the SRC at 1530 m ASL, roughly three-quarters of the distance from the canyon bottom to the ridgetop. These sensors were chosen because they appeared to be the least influenced by the terrain and most representative of the gradient level winds. Threshold velocities of 6 and 5 m s⁻¹ were chosen for BSB and SRC, respectively (Fig 43). 83% and 80% of the data fell below these threshold speeds at BSB and SRC, respectively. Speeds below these thresholds fall within the range of diurnal wind flows reported in the literature (Horst and Doran, 1986) and visual inspection of the vector maps further confirmed this choice of threshold wind speeds, as all four regimes were clearly identified by the surface flow patterns at each site.

After filtering out the synoptically driven periods, the remaining data were then partitioned into regimes (1) to -(3) based on visual inspection of the hourly vector maps. Periods which exhibited clearly defined downslope flow were partitioned into regime (1). Periods which exhibited clearly defined upslope flow were partitioned into regime (2). And afternoon periods during which the upslope regime was disturbed were partitioned into regime (3). Transition periods from one regime to another were also identified based on visual inspection of the hourly vector maps.

The NOAA-FRD mesonet sensor at the summit of BSB (Fig. 1a, SUM) as well as archived North American Mesoscale Model (NAM) forecasts were reviewed for indications of upper-level flows that may have been decoupled from surface measurements. References in the text to upper-level or gradient-level winds refer to flows from these data sources.

4.2 Data Averaging

Surface wind observations were averaged over a 10-min period at the top of each hour to represent an average speed valid at the top of each hour. This averaging scheme was chosen to be representative of wind speeds from NWP forecasts. Although NWP output is valid at a particular instant in time, there is some inherent averaging in these ‘instantaneous’ predictions. The averaging associated with a given prediction depends on the time-step and grid spacing used in the NWP model, but is typically on the order of minutes. The 10-min averages are referred to in the text as ‘hourly’ data.

Hourly vector maps were used to visualize the spatial patterns of the wind fields for classifying flow regimes. The vector maps were produced by partitioning the hourly data into one of two categories: (1) strong synoptic forcing or (2) weak synoptic forcing (i.e., diurnal winds dominate), and then averaging the hourly data (for each sensor) within each category over the entire monitoring period. The result is an hourly average wind vector at each sensor location for each flow category. For example, a vector map for 1300 hours under weak synoptic forcing would be produced by filtering out the periods of strong synoptic forcing and then averaging all hourly flow data for the 1300 hour at each sensor over the entire monitoring period. Partitioning of data into weak vs. strong synoptic forcing was described in Section 4.1.

All data analysis and visualization was performed in R (R Core Team, 2013). Vector maps were produced using the ggmap library (Kahle and Wickam, 2013) and diurnal wind contour plots were produced using the metvurst library (Salabim, 2013).

5 Results and Discussion

Results for BSB are presented in section 5.1. Results for SRC are presented in section 5.2. Average flows for the diurnal wind regimes are presented for each site and then the disturbance to the diurnal wind regime by synoptic-scale forcing is described. Transitions within the diurnal wind regime (e.g., upslope to afternoon regime) occurred at roughly the same time of day throughout the monitoring periods, with no discernible differences between average hourly vector maps for the first and second half of the monitoring period. Thus, results for diurnal winds are reported as averages for the entire monitoring period. This is reasonable since monitoring periods were during summertime conditions at both sites. ~~All times are reported as local daylight time.~~

5.1 BSB

5.1.1 Diurnal Winds: Upslope, Afternoon, and Downslope Regimes

Diurnal slope winds are driven by solar-induced horizontal temperature gradients between the ground surface and the air. Whiteman (2000) provides a thorough discussion of diurnal mountain winds. The diurnal wind regime for an isolated mountain is typically characterized by upslope winds during the day due to local solar heating of the surface and downslope winds at night due to local surface cooling. An afternoon,

or coupled, regime often develops when gradient level winds become mixed in with the growing surface layer. There is a transition phase between each phase of the diurnal cycle as the temperature structure of the atmosphere responds and adjusts to the changing incident solar radiation at the surface. The daily cycle can be disturbed by interference from larger-scale winds.

Sunrise ranged from 0600 to 0700 during the monitoring period. Upslope winds formed between 0800 and 0900 and the upslope regime was fully established by 1000 and persisted until around 1200. Upslope winds peaked around 1100. This regime was characterized by thermally-driven upslope winds on all sides of the butte flowing up from the surrounding SRP (Fig 45). The timing of onset and occurrence of peak winds in the upslope regime was consistent with Banta and Cotton (1982) and Geerts et al. (2008), who reported peaks in upslope flow before local solar noon (LSN) for relatively small mountains. Others have reported later peaks in upslope flow after LSN for larger mountain ranges (McNider and Pielke, 1981; Reiter and Tang, 1984). Geerts et al. (2008) discussed this discrepancy in the reported timing of upslope flows for different mountain ranges and described the development of upslope winds as scaling with the size of the mountain. BSB is a relatively small isolated mountain (by Geerts et al. (2008) terminology; horizontal scale of ~5 km and vertical scale of ~800 m above the surrounding SRP), and so establishment of the upslope regime prior to LSN fits with this scaling theory. Upslope flows persisted about two hours longer than those at the South Park site in Colorado reported by Banta and Cotton (1982). This difference could be attributed to the upwind terrain, as westerly flows from the Rocky Mountains at the South Park Site were likely more turbulent than the southwesterly flows approaching BSB from the SRP, and perhaps were able to more quickly entrain the developing convective boundary layer (CBL) at South Park.

Wind speeds in the upslope regime ranged from 1.8 to 7.3 m s⁻¹, with an average of 3.1 m s⁻¹ (Table 3). There were a few ridgetop sensors which appeared to be decoupled from the diurnal flow regime on the butte (discussed in detail at the end of this section); if these sensors are removed, the wind speeds ranged from 1.8 to 4.5 m s⁻¹, with an average of 3.0 m s⁻¹. These are higher speeds than those reported by Geerts et al. (2008), but similar to the range reported by Banta and Cotton (1982). Differences in the reported range of speeds between this study and Geerts et al. (2008) could be attributed to differences in the actual quantities reported. Geerts et al. (2008) used an averaging scheme to calculate a mean anabatic wind that is a function of the circumference of the polygon obtained by connecting the midpoints between observation stations around the mountain. Also, their wind measurements were made at 10 m AGL, while ours were made at 3.3 m AGL. Upslope wind speeds were typically higher further up the slopes than lower on the butte (Fig. 65a; Fig 76). Ridgetop sensors also appeared to be less coupled with the diurnal flow regime on the butte and more correlated with the large-scale flows; this is confirmed by contour plots of wind direction over time (Fig. 76) and is discussed in further detail at the end of this section.

Upslope winds transitioned to the afternoon regime between 1200 and 1300. This transition is most notable by an increase in wind speeds on the southwest side of the butte and a shift in the wind directions on the northeast side of the butte (Fig. 45). This regime included local flows that generally correlated with the gradient level winds above the ridgetops due to convective mixing in the deep afternoon boundary

layer. Convective mixing was fully established by 1400 [hours](#) and persisted until around 2000 [hours](#). Wind speeds peaked around 1500 [hours](#) and were fairly consistent through 1900 [hours](#). The onset of the afternoon regime was slightly later in the day than that reported by Banta and Cotton (1982) which could be due to less turbulent approach flow at BSB as discussed above. During the afternoon regime, the prevailing southwesterly flow was routed around the northwest and southeast sides of the butte (e.g., sensors R9 and R13). Wind speeds were highest on the ridgetops and southwest slopes and lowest on the northeast slopes (Fig. [45](#)). There was some apparent recirculation on the northeast side of the butte as well as in some of the side drainages (Fig. [45](#)). Wind speeds in the afternoon regime ranged from 2.3 m s⁻¹ to 8.1 m s⁻¹ with an average of 4.1 m s⁻¹.

Sunset ranged from 2030 to 2130 [hours](#) during the monitoring period. The afternoon regime began to decay and transition into downslope winds between 2100 and 2200 [hours](#). The downslope regime was fully established by 2300 and persisted until around 0800 [hours](#). Peak downslope winds occurred around 0000 [hours](#). The timing of onset and occurrence of peak winds in the downslope regime agreed with observations reported in Banta and Cotton (1982). Downslope flows are clearly shown in the hourly vector plots, with flows going from the top of the butte down all side drainages around the butte and flowing out onto the SRP (Fig. [45](#)). Wind speeds in the downslope regime ranged from 1.3 to 12.0 m s⁻¹, with an average of 3.7 m s⁻¹. If the decoupled ridgetop sensors are removed, the range was 1.3 to 7.5 m s⁻¹, with an average of 3.4 m s⁻¹ (Table 3). This range is similar to that reported in Banta and Cotton (1982) and slightly larger than that reported in Horst and Doran (1986). Others have proposed an acceleration of flow with downslope distance due to thickening of the katabatic layer from entrainment of ambient air into the slope flow and increased buoyancy deficit with downslope distance (Horst and Doran, 1986); however, we did not observe a consistent trend in wind speed with location on the slope (low vs. high) during the downslope regime (Fig. [65b](#)).

Diurnal winds dominated the local flows on and around the butte under periods of weak synoptic forcing. During these periods, flow on and around BSB was decoupled from the large-scale atmospheric flows, except for high elevation ridgetop sensors (R26, R35, TSW7) and one exposed mid-elevation ridge sensor (R15). This decoupling is evident from the vector maps (Fig. [45](#)) and is also confirmed by the contour plots which show that these ridgetop locations do not experience the strong diurnal shifts in wind direction that other locations on and around the butte experience (Fig. [67](#), [78](#)). This ridgetop decoupling likely occurred because these locations were high enough in the atmosphere to protrude out of the nocturnal boundary layer (NBL) and the morning-time developing shallow CBL. Thus, the ridgetop winds were coupled with the large-scale flows during all periods of the day. During nighttime hours the ridgetop locations would experience residual layer winds and would only be coupled with the rest of the flow on and around the butte once the residual layer was entrained by the growing shallow CBL and the convective mixing regime was fully established. This proposed structure is confirmed by the vector plots, which show that ridgetop winds did not change much from one regime to the next and only correlated with winds at other nearby locations on the butte during the convective mixing regime (Fig. [45](#)).

5.1.2 Synoptic Disturbance of Diurnal Winds

Under periods of strong synoptic forcing, such as the passage of a cold front, the diurnal wind regime was disrupted and a synoptically-forced regime persisted. Two types of flow events occurred within the synoptically-forced regime, one with southwesterly flow and one with northeasterly flow (Fig. 89). The diurnal slope flows on BSB were completely overtaken by the larger scale flows in this regime (Fig 8-9 vs. Fig. 45). During these events, daytime winds were consistently from the southwest, but in a few cases, during nighttime and early morning hours, winds were from the northeast (Fig. 89).

The southwest flows are referred to as 'synoptically driven upvalley' flows and the northeasterly flows are referred to as 'synoptically driven downvalley' flows. Synoptically driven upvalley flows were generally associated with the passage of cold fronts from the west/southwest. Evolution of the synoptically driven downvalley flows is more complex and some potential mechanisms are described below. Wind speeds during the synoptically driven upvalley flows ranged from 2.9 to 20.3 m s⁻¹, with an average of 7.1 m s⁻¹; the downvalley flow speeds ranged from 0.1 to 24.4 m s⁻¹, with an average of 6.0 m s⁻¹. The synoptically driven downvalley (northeasterly) flows occurred less frequently than the synoptically driven upvalley (southwesterly) flow events; however, 4 distinct nighttime northeasterly flow events were observed during the monitoring period.

There are at least three potential mechanisms which may have contributed to the synoptically driven downvalley events that we observed. One mechanism is related to the SPCZ described in section 2.1. Mechanical channeling of the gradient level winds by the surrounding terrain to the north and strong southwesterly flows on the SRP can create an SPCZ-like convergence zone with strong upvalley winds to the south of the zone and strong downvalley winds to the north of the zone. Winds at BSB could be southwesterly or northeasterly depending on which side of the convergence zone it was on. A second mechanism is based on observations from the NOAA-FRD mesonet suggesting that during summer months SPCZ-like events occur in association with the passage of fronts or thunderstorm activity in the mountains to the north. The former will often generate strong outflows through the northern valleys onto the SRP, and the latter will sometimes generate outflow gust fronts. A third possibility is that surface pressure gradients, in some cases, may have contributed to the northeasterly flows. Two of the observed synoptically driven down valley flow events occurred during periods where there was a strong northeast to southwest surface pressure gradient which could have facilitated the flow; however, the other two observed synoptically driven downvalley events did not occur during periods of favorable surface pressure gradients, so although surface pressure may be an influence, it was not the sole cause of these strong downvalley flow events. It is possible that any of these three mechanisms may have contributed to the observed downvalley flows on BSB.

It is interesting that during periods of synoptically driven downvalley flows wind speeds were generally higher on the southwest (leeward) side of BSB than on the northeast (windward) side. Perhaps this is because the maximum in the synoptically driven downvalley flow occurred at some higher elevation and was not well-mixed with near-surface winds due to nighttime temperature stratification in the NBL. This stratified flow could have become mixed into the surface flow at the ridgetops and

pulled down the southwest side of BSB. The northeasterly flow also would have been enhanced by the nighttime downslope flow on the southwest side of BSB, thus producing stronger winds on this side as compared to the northeast (windward side), where the downslope flow would be in opposition (southwesterly) to the northeasterly flow.

5.2 SRC

5.2.1 Diurnal Winds: Upslope, Afternoon, and Downslope Regimes

The diurnal wind regime for a canyon or valley is similar to that of the isolated mountain, with upslope/upvalley winds during the day due to local solar heating of the surface and downslope/downvalley winds at night due to local surface cooling. However, the afternoon, or coupled, regime often does not develop in deep or narrow canyons due to strong atmospheric decoupling of the canyon flows from the upper level winds (Banta and Cotton, 1982).

Sunrise ranged from 0500 to 0630 hours during the monitoring period at SRC. Upslope winds formed around 0900 hours and were fully established by 1000 hours, peaked around 1200 hours and persisted until around 1500 hours. The upslope regime was characterized by thermally-driven upslope winds on both sides of the canyon as well as up smaller side drainage slopes (Fig. 910). The one notable exception was sensor NM2, which experienced easterly or southeasterly flow during most periods of the day (Fig. 910). We believe this sensor was perhaps located in a local recirculation zone formed in the small side drainage; this is discussed at the end of this section. Wind speeds in the upslope regime ranged from 0.75 to 4.0 m s⁻¹, with an average of 2.4 m s⁻¹ (Table 3).

Wind speeds tended to be highest at the upper elevation sensors around the onset of the upslope regime at 0900 hours (Fig. 4011). As the upslope regime developed, wind speeds peaked around 1100 and were highest at the mid elevation sensors (Fig. 4011) and this trend continued through 1300. The NW and SE transects do not follow these trends. The NW transect had consistently lower speeds at the mid elevation sensor during all periods of the upslope regime. This could be because NW3 was located slightly off of the ridge on a northwest aspect and perhaps decoupled from the flow along the rest of the NW transect. The SE transect had consistently higher speeds at the mid elevation sensor (SE4). The higher speeds at SE4 could be because this sensor was located on a ridge exposed to a prominent side drainage (Lake Creek) just to the east of our study area (~~Fig. 1~~). Flows out of this Lake Creek drainage could have influenced this sensor more than others along the SE transect due to its location on the ridge and steep terrain to the southeast (Fig. 34).

We did not observe afternoon convective mixing at SRC as we did at BSB. This is consistent with Banta and Cotton (1982) who noted that a true convective mixing regime is not well documented in narrow mountain canyons, likely due to the strong channeling effect exerted by the canyon on the flow. The afternoon regime at SRC was characterized by a change from upslope to upvalley winds around 1500. This afternoon upvalley regime was fully established by 1600 and persisted through 1900. The most notable change between the upslope regime and the afternoon regime was

the shift in wind direction from up the canyon walls (northerly or southerly flow) to upriver (westerly flow), especially for the lower elevation sensors. Daytime gradient level winds were typically from the west (upriver winds), so it could be difficult to determine if this afternoon shift in wind direction was driven by convective mixing of gradient level winds down into the canyon or the formation of thermally-driven upvalley flow within the canyon. The fact that this change in wind direction was most notable in the lower elevation sensors (Fig. 910) points to a thermally-driven mechanism. Wind speeds were fairly consistent throughout this time period and ranged from 0.92 to 4.2 m s⁻¹, with an average of 2.5 m s⁻¹ (Table 3). Wind speeds were the lowest near the canyon bottom except for the SE and NW transects, which had the lowest speeds at high and mid elevation sensors (SE3 and NW3). Both of these sensors were located slightly off of the main ridge. It is interesting that the lowest sensors responded most noticeably to the shift from upslope to upvalley flow with a change in wind direction, but that the highest speeds were still observed at the upper elevation sensors.

Sunset ranged from 1900 to 2030 hours during the monitoring period. Upvalley flow began to weaken and transition to downslope flow between 2000 and 2100. The downslope regime was fully established by 2200 and persisted until around 0700. Peak wind speeds in the downslope regime occurred around 2200. Wind speeds in the downslope flow regime ranged from 0.33 to 4.1 m s⁻¹, with an average of 1.2 m s⁻¹ (Table 3). Wind speeds tended to increase with upslope distance (Fig. 142), with the exception of the SE transect, likely due to the location of SE3 and SE4 as discussed above. This trend was consistent throughout the duration of the downslope regime.

Diurnal trends were further inspected for the NM transect because it was not located near any prominent side drainages and likely exhibited the simplest flow characteristics. Contour plots show a strong diurnal signal for all sensors in this transect (Fig. 132), indicating that diurnal flows are a major flow feature in the SRC. Winds were from the east/southeast in the early morning and from the west/northwest in the afternoon and the highest speeds occurred at the upper elevation sensors during early morning hours. One exception was the NM2 sensor, which rarely experienced winds from the west/northwest and did not experience a morning time peak in wind speed. This sensor was located slightly off of a mid-slope ridge on a slope with a northwest aspect. We suspect that this location was possibly a zone of recirculation. The lowest sensor, NM4, also did not experience a morning peak in wind speed and rarely experienced winds from the northeast. The highest speeds occurred during periods of synoptic disturbance, which we believe had more of an effect at upper elevations in the SRC than lower ones near the river bottom. This is discussed further in the next section.

5.2.2 Synoptic Disturbance of Diurnal Winds

Two types of synoptic disturbances to the diurnal wind regime in the SRC were observed (Fig. 4314). One is associated with the passage of frontal systems from the west, which brings strong westerly gradient winds. The other appears to be associated with the presence of an east-west pressure gradient that generates strong morning-time easterly flow. During the passage of frontal systems, westerly winds are

channeled up the river canyon and most sensors in SRC (with the exception of those located in side drainages) experienced westerly flow. These events tended to occur during mid-afternoon hours. Wind speeds during this type of synoptic disturbance ranged from 2.1 to 5.7 m s⁻¹, with an average of 3.8 m s⁻¹.

The highest observed wind speeds in the SRC were from the east during morning hours (Fig. 4213, 4314). Wind speeds during these pressure-driven downvalley events ranged from 0.84 to 9.1 m s⁻¹, with an average of 3.1 m s⁻¹. These events occurred roughly every few days and appeared to be induced by a surface pressure gradient formed when a thermal trough existed on the Columbia Plateau to the northwest of SRC and high pressure existed to the east of SRC (Fig. 154). An east-west surface pressure gradient existed on days when enhanced downvalley flow was observed. On days when the downvalley flow feature was not observed, there was no east-west surface pressure gradient. The highest wind speeds during this type of flow event were observed at the upper elevations of the SRC (Fig. 165). The east-west surface pressure gradient coupled with the typical nighttime/early morning katabatic flow in the canyon resulted in very strong downvalley winds in the SRC. This pressure-enhanced katabatic surface flow tended to be decoupled from the larger-scale gradient flow (which is typically from the west) during these pressure-driven events.

5.3 Archived Data

All data are archived as downloadable SQLite databases. Access to these databases along with tools to query, process, and visualize, the data is described at <http://www.firemodels.org/index.php/windninja-introduction/windninja-publications>. Descriptions of the NOAA mesonet data and contact information regarding mesonet data are found at <http://www.noaa.inel.gov/capabilities/mesonet/mesonet.htm> and <http://niwc.noaa.inel.gov/> and <http://niwc.noaa.inel.gov/>.

(6)

6 Conclusions

We have presented an analysis of two high-resolution surface wind datasets, one collected from a tall isolated mountain, and the other from a steep river canyon. The wind data were ~~analyzed~~analysed and presented in terms of four flow regimes: upslope, afternoon, downslope, and a synoptically-driven regime. These datasets constitute a unique inventory of surface wind measurements at very high spatial resolution under dry summertime conditions. Public access to the archived datasets has been described.

Surface winds on and around BSB were completely decoupled from large-scale flows during upslope and downslope flow regimes, except for the highest elevation ridgetop sensors. These ridgetop locations at BSB tended to correlate better with gradient-level winds than with the local diurnal surface flows. Surface winds in SRC were decoupled from large-scale flows except during periods of strong synoptic forcing that enhanced either upriver or downriver flows.

Wind speeds increased with distance upslope during the upslope regime at BSB, but generally decreased with distance upslope at SRC. Wind speed did not have a simple, consistent trend with position on the slope during the downslope regime at

BSB, but generally increased with distance upslope at SRC. We did not observe a convective mixing regime at SRC under periods of weak synoptic forcing, only a transition from upslope to thermally-driven upriver flow.

The highest speeds measured at BSB occurred during the passage of frontal systems which generated strong southwesterly flows and during infrequent strong northwesterly flows presumably generated through SPCZ-like dynamics, thunderstorm outflows, or surface pressure gradients. Ridgetop winds were often twice as high as surface wind speeds measured on the surrounding SRP. The highest speeds measured at SRC occurred during late morning hours and were from easterly flows presumably produced by surface pressure gradients induced by formation of a thermal trough over the Columbia Plateau to the NW and high pressure to the east. The highest wind speeds during these pressure-driven easterly flow events were measured at the mid to high elevation sensors.

These results have important implications for modeling near-surface winds in complex terrain. The fact that surface winds at both sites tended to be decoupled from large-scale flows under periods of weak synoptic forcing suggests that traditional operational weather model winds (i.e., with numerical grid resolutions of around 4 km or larger) are not likely to be good predictors of local winds in sub-grid scale complex terrain. Under periods of strong synoptic forcing, variability in surface winds was sufficiently large due to terrain-induced mechanical effects (speed-up over ridges and decreased speeds on leeward sides of terrain obstacles), that a mean wind for a 4 km grid cell encompassing these terrain features would not be representative of actual surface winds at most locations on or within the terrain feature. The findings from this work along with the additional archived data and available mesonet data at BSB should provide guidance for future development and evaluation of high-resolution wind models and integrated parameterizations, such as for simulating diurnal slope flows and non-neutral atmospheric stability effects.

Acknowledgements

The Department of Interior Bureau of Land Management Idaho Falls, ID field office facilitated the field campaign and Barry Sorenson provided critical advice on local conditions, access roads, and weather as well as permission to store equipment on-site during the deployment at Big Southern Butte. Thanks to Nicole Van Dyk, Olga Martyusheva, Jack Kautz, Peter Robichaud, and Ben Kopyscianski of the Rocky Mountain Research Station for help with the field installation and maintenance at the Salmon River site. Funding was provided by the Joint Fire Science Program, the US Forest Service, Washington State University, and the National Oceanic and Atmospheric Administration Field Research Division.

References

- Andretta, T.A., 2002. Climatology of the Snake River Plain convergence zone. *National Weather Digest*. 26, 37–51.
- Andretta, T.Z., Hazen, D.S., 1998. Doppler radar analysis of a Snake River Plain convergence event. *Weather and Forecasting*. 13, 482–491.
- Banta, R.M., 1984. Daytime boundary-layer evolution over mountainous terrain. Part 1: observations of the dry circulations. *Mon. Wea. Rev.* 112, 340–356.
- Banta, R.M., Cotton, R., 1982. An analysis of the structure of local wind systems in a broad mountain basin. *J. Appl. Meteorol.* 20, 1255–1266.
- Beaucage, P., Brower, M.C., Tensen, J., 2012. Evaluation of four numerical wind flow models for wind resource mapping. *Wind Energy*.
- Berg, J., Mann, J., Bechmann, A., Courtney, M.S., Jørgensen, H.E., 2011. The Bøllund Experiment, Part I: Flow over a steep, three-dimensional hill. *Boundary-Layer Meteorol.* 141, 219–243.
- Chrust, M.F., Whiteman, C.D., Hoch, S.W., 2013. Observations of thermally driven wind jets at the exit of Weber Canyon, Utah. *J. Appl. Meteorol. Climatol.* 52, 1187–1200.
- Daly, C., Conklin, D.R., Unsworth, M.H., 2010. Local atmospheric decoupling in complex topography alters climate change impacts. *Int. J. Climatol.* 30, 1857–1864.
- [Defant, F. 1949. "Zur Theorie der Hangwinde, nebst Bemerkungen sur Theorie der Berg- und Talwinde." Archiv fuer Meteorologie Geophysik und Bioklimatologie Ser. A.\(1\): 421-450.](#)
- Forthofer, J., Shannon, K., Butler, B., 2009. Simulating diurnally driven slope winds with WindNinja. Eighth Symposium on Fire and Forest Meteorology. Oct 13-15. Kalispell, MT.
- Forthofer, J.M., Butler, B.W, Wagenbrenner, N.S., In [ReviewPress](#). A comparison of two approaches for simulating fine-scale winds in support of wildland fire management: Part 1 – model formulation and comparison against measurements. *Int. J. Wildland Fire*.
- Geerts, B., Miao, Q., Demko, J.C., 2008. Pressure perturbations and upslope flow over a heated, isolated mountain. *Mon. Wea. Rev.* 136: 4272–4288.
- Grell, G.A., Emeis, S., Stockwell, W.R., Schoenemeyer, T., Forkel, R., Michalakes, J., Knoche, R., Seidl, W. 2000. Application of a multiscale, coupled MM5/chemistry model to the complex terrain of the VOTALP valley campaign. *Atmos. Environ.* 34, 1435–1453.
- Horst, T.W., Doran, J.C., 1986. Nocturnal drainage flow on simple slopes. *Boundary-Layer Meteorol.* 34: 263–286.
- Jiménez, P., Jorba, O., Parra, R. Baldasano, J.M., 2006. Evaluation of MM5-EMICAT2000-CMAQ performance and sensitivity in complex terrain: high-resolution application to the northeastern Iberian peninsula. *Atmos. Environ.* 40, 5056–5072.

719 Jiménez, P., Dudhia, J., 2012. Improving the representation of resolved and unre-
720 solved topographic effects on surface wind in the WRF model. *J. Appl. Meteorol.*
721 *Climatol.* 51, 300–316.

722 Kahle, D., Wickham, H., 2013. ggmap: A package for spatial visualization with
723 Google Maps and OpenStreetMap. R package version 2.3. [http://CRAN.R-](http://CRAN.R-project.org/package=ggmap)
724 [project.org/package=ggmap](http://CRAN.R-project.org/package=ggmap).

725 Langhans, W., Juerg, S., Fuhrer, O., Bieri, S., Schär, C., 2013. Long-term simulations
726 of thermally driven flows and orographic convection at convection-parameterizing
727 and cloud-resolving resolutions. *J. Appl. Meteor. Climatol.* 52, 1490–1510.

728 Lundquist, K.A., Chow, F.K., Lundquist, J.K., 2010. An immersed boundary method
729 for the Weather Research and Forecasting Model. *Mon. Wea. Rev.* 138:796–817.

730 McNider, R.T., Pielke, R.A., 1981. Diurnal boundary-layer development over sloping
731 terrain. *J. Atmos. Sci.* 38: 2198–2212.

732 Palma, J.M.L.M., Castro, F.A., Ribeiro, L.F., Rodrigues, A.H., Pinto, A.P., 2008. Line-
733 ar and nonlinear models in wind resource assessment and wind turbine micro-
734 siting in complex terrain. *J. Wind Engineer. Indust. Aerodynam.* 96, 2308–2326.

735 R Core Team, 2013. R: A language and environment for statistical computing. R
736 Foundation for Statistical Computing, Vienna, Austria. URL [http://www.R-](http://www.R-project.org/)
737 [project.org/](http://www.R-project.org/).

738 Reiter, E.R., Tang, M., 1984. Plateau effects on diurnal circulation patterns. *Mon.*
739 *Wea. Rev.* 112: 638–651.

740 Rothermel, R.C., 1972. A mathematical model for predicting fire spread in wildland
741 fuels: Ogden, UT, p. 40.

742 Salabim, T., 2013. Metvurst: meteorological visualization utilities using R for science
743 and teaching. URL <https://github.com/tim-salabim/metvurst>.

744 Scire, J.S., Robe, F.R., Fernau, M.E., Yamartino, R.J., 2000. A user's guide for the
745 CALMET meteorological model. Earth Tech, Inc.: Concord, MA.

746 Sharples, J.J., McRae, R.H.D., Wilkes, S.R., 2012. Wind-terrain effects on the propa-
747 gation of wildfires in rugged terrain: fire channeling. *Intern. J. Wild. Fire.* 21, 282–
748 296.

749 Simpson, C.C., Sharles, J.J., Evans, J.P., McCabe, M.F., 2013. Large eddy simula-
750 tion of atypical wildland fire spread on leeward slopes. *Intern. J. Wild. Fire.* 22,
751 599–614.

752 Taylor, PA, Teunissen, HW (1987.) The Askervein Hill Project: Overview and back-
753 ground data. *Boundary-Layer Meteorology* 39, 15-39.

754 Wagenbrenner, N.S., Lamb, B.K., Forthofer, J.M., Shannon, K.S., Butler, B.W., In
755 preparation. Effect of model horizontal grid resolution on near-surface wind pre-
756 dictions in complex terrain: evaluations with high-resolution field observations
757 from an isolated mountain and a steep river canyon. To be submitted to *J. Appl.*
758 *Meteorol. Climatol.*

759 Whiteman, C.D. 2000. Mountain Meteorology: Fundamentals and Applications. Ox-
760 ford University Press. New York.

761 Zardi, D., Whiteman, CD (2013) Diurnal Mountain Wind Systems. In 'Mountain
762 Weather Research and Forecasting.' (Eds FK Chow, SFJ De Wekker, BJ Snyder.)
763 pp. 35-119. Springer Netherlands. Chap 2

764 Zhong, S., Fast, J., 2003. An evaluation of MM5, RAMS, and Meso-Eta models at
765 subkilometer resolution using VTMX field campaign data in the Salt Lake valley.
766 Monthly Weather Review. 131, 1301–1322.
767

768 Table 1. Sonic anemometer and vertical profiling sensor details.

ID	Site ¹	Sensor	Model	Time Period	Averaging Period
WSU1	BSB	Sodar	Scintech	14 Jul–15 Jul 2010	30-min
		Sonic	ATI	14 Jul–18 Jul 2010	10 Hz
WSU2	BSB	Sodar	Scintech	15 Jul–19 Jul 2010	30-min
				31 Aug–1 Sep 2010	30-min
NOAA1	BSB	Sodar	Radian 600PA	14 Jul–19 Jul 2010	30-min
		Radar	Radian 3000	LAP-14 Jul–19 Jul 2010	30-min
NOAA2	BSB	Sodar	ASC 4000	14 Jul–19 Jul 2010	30-min
ST1	SRC	Weather station	Viasala, WXT	16 Aug–12 Sep 2011	15-min
		Sonic	CSAT3	18 Aug–19 Aug 2011	10 Hz
ST2	SRC	Sodar	Scintech	16 Aug–18 Aug 2011	30-min
				29 Aug–31 Aug 2011	30-min
		Sonic	ATI	16 Aug–18 Aug 2011	10 Hz
ST3	SRC	Weather station	Viasala, WXT	17 Aug–12 Sep 2011	15-min
ST4	SRC	Sonic	ATI	16 Aug 19–Aug 2011	10 Hz

¹BSB = Big Southern Butte; SRC = Salmon River Canyon.

771 | Table 2. Radiosonde launches at BSB and SRC. Times are localLT.

Site ¹	Date	Time of launch
BSB	August 31 2010	16:57
	September 1 2010	16:59
	September 2 2010	10:35
SRC	July 18 2011	11:28
		13:56
		15:50
		18:14
		20:00
		21:32

772 | ¹ BSB = Big Southern Butte; SRC = Salmon River Canyon.
773

774 Table 3. Measured wind speeds (m s^{-1}) during upslope, downslope, and convective
 775 mixing regimes at Big Southern Butte (BSB) and Salmon River Canyon (SRC).
 776 Decoupled ridgetop locations (sensors R26, R35, TSW7, and R15) were omitted from
 777 BSB averages; speeds in parentheses include ridgetop sensors.

Site	Wind Speed	Upslope (1100 LT)	Afternoon (1600 LT)	Downslope (0000 LT)
BSB ¹	Min (m s^{-1})	1.8	2.3	1.3
	Max (m s^{-1})	4.5 (7.3)	8.1	7.5 (12.0)
	Mean (m s^{-1})	3.0 (3.1)	4.1	3.4 (3.7)
SRC ¹	Min (m s^{-1})	0.75	0.92	0.33
	Max (m s^{-1})	4.0	4.2	4.1
	Mean (m s^{-1})	2.4	2.5	1.2

778 ¹ BSB = Big Southern Butte; SRC = Salmon River Canyon
 779

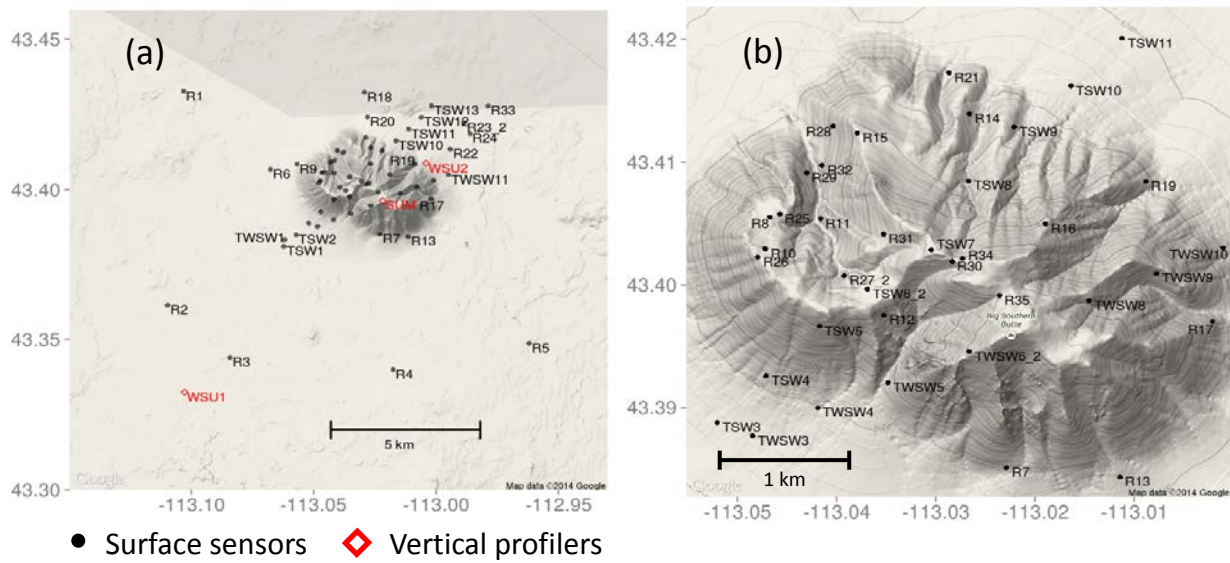
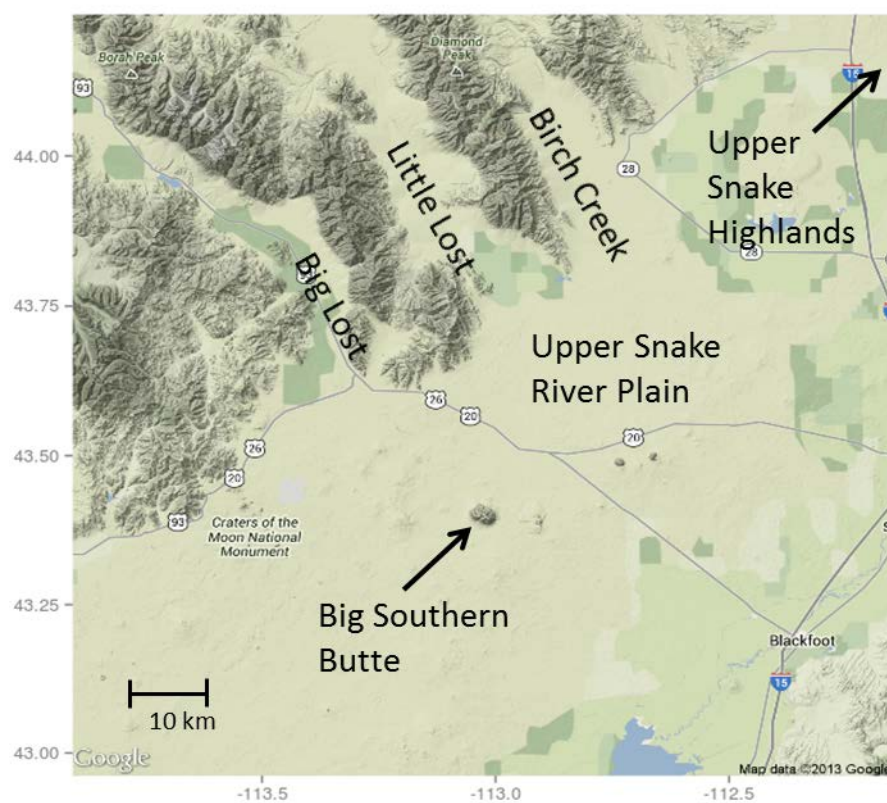


Fig. 1. Site overview and sensor layouts at the Big Southern Butte (a, b). Black circles indicate surface sensors. Red diamonds indicate sonic anemometers and vertical profiling sensors.



788 Fig. 2. Snake River Plain and prominent drainages surrounding the Big Southern
 789 Butte study site. The topographical gradient is increasing in elevation from south to
 790 north. Elevation of plain around Big Southern Butte is nominally 1585 m.
 791

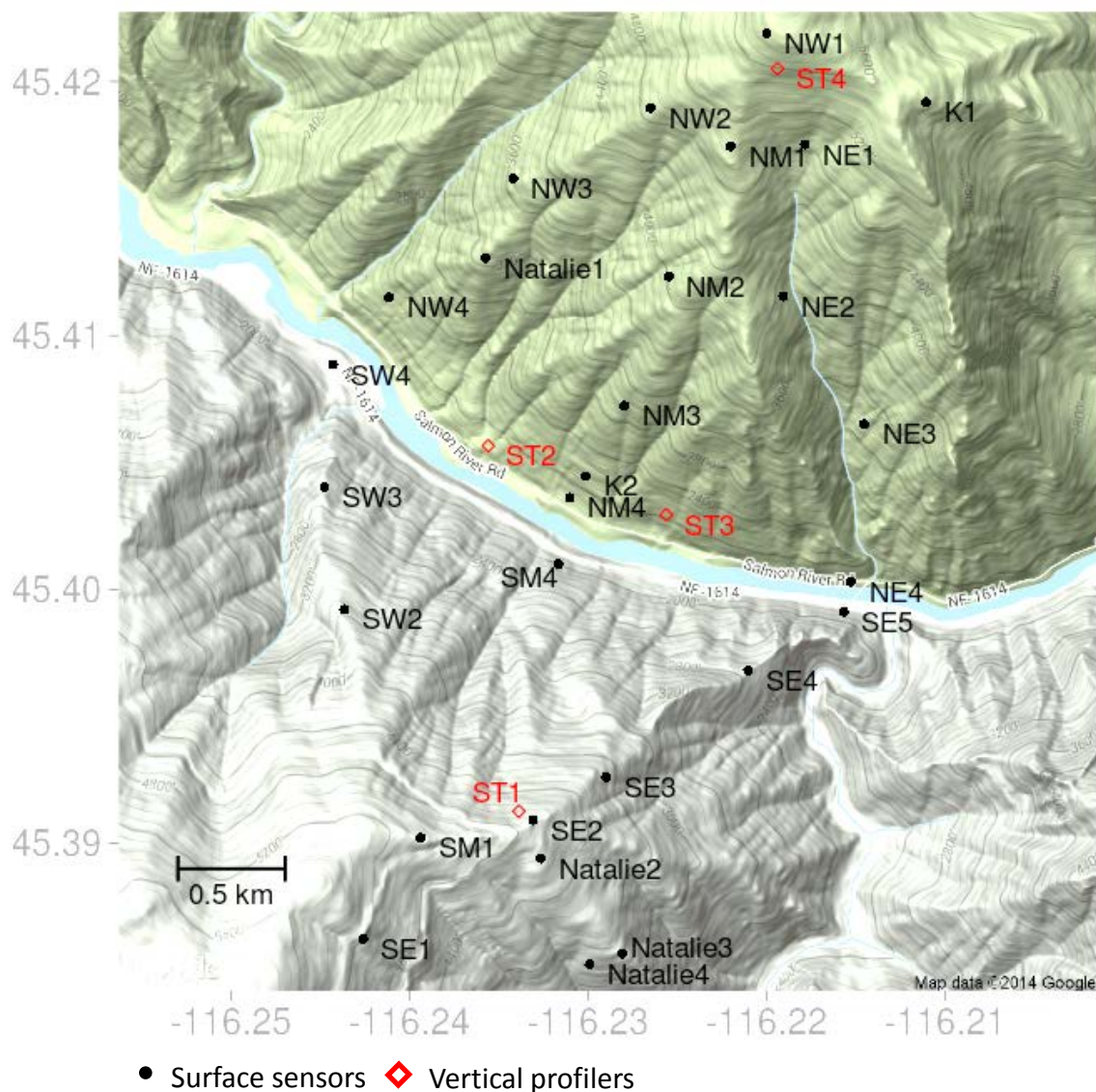


Fig. 3. Site overview and sensor layouts at the Salmon River Canyon. Black circles indicate surface sensors. Red diamonds indicate sonic anemometers and vertical profiling sensors. The topographical gradient is increasing in elevation from left to right. Elevation of river is 540 m.

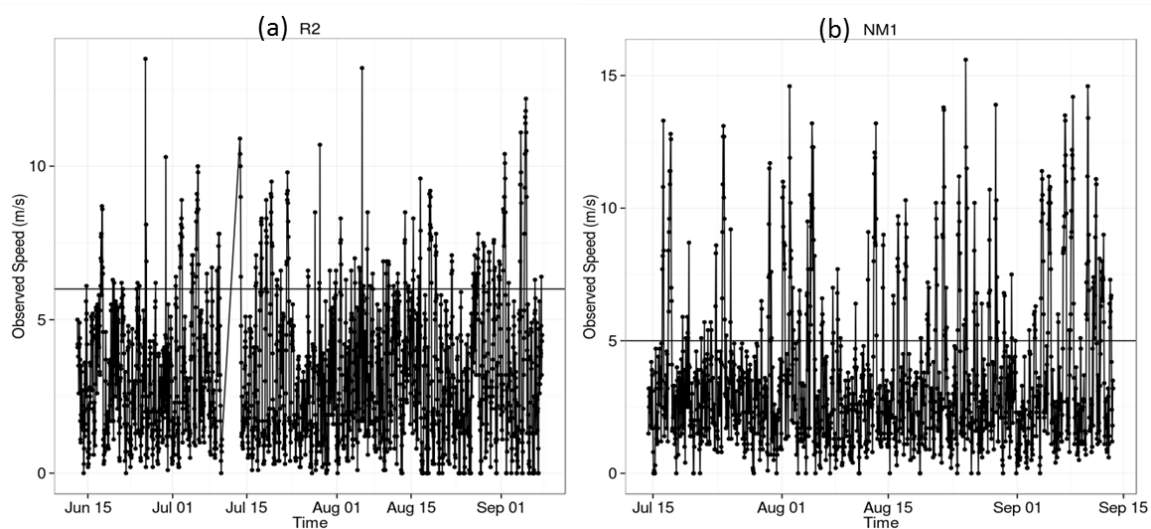


Fig. 4. Observed hourly wind speeds for sensor R2 at Big Southern Butte (elevation 1560 m) and NM1 (elevation 1734 m) at the Salmon River Canyon study site. The horizontal line indicates the threshold speed chosen to partition synoptically driven events from diurnal events.

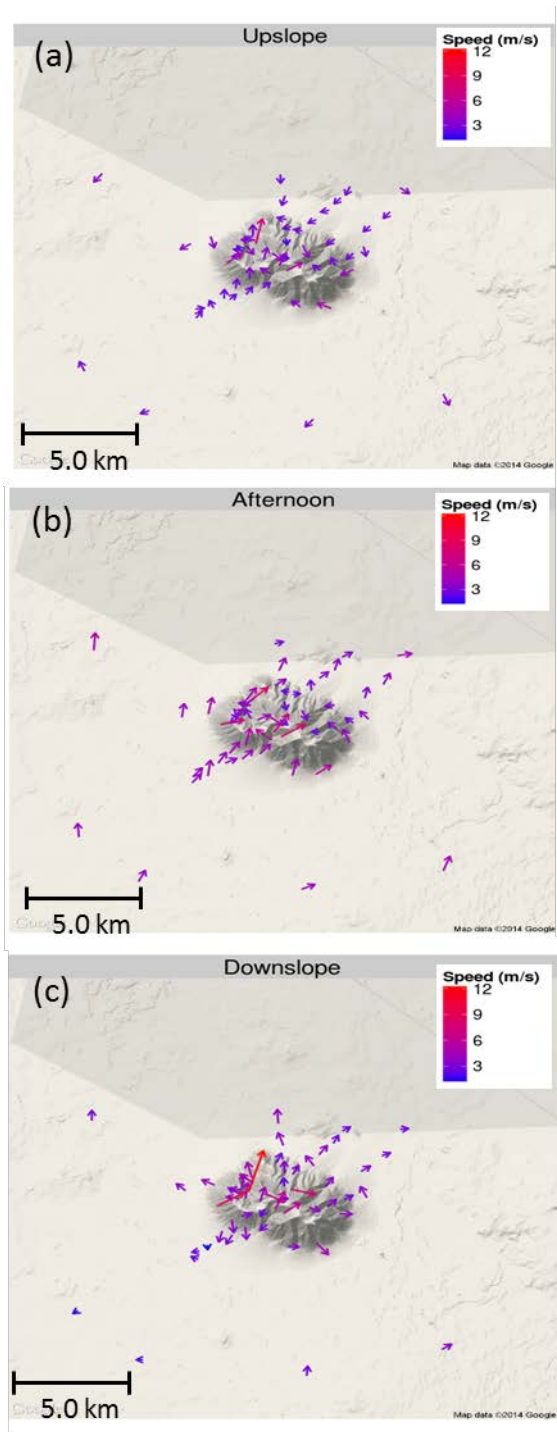
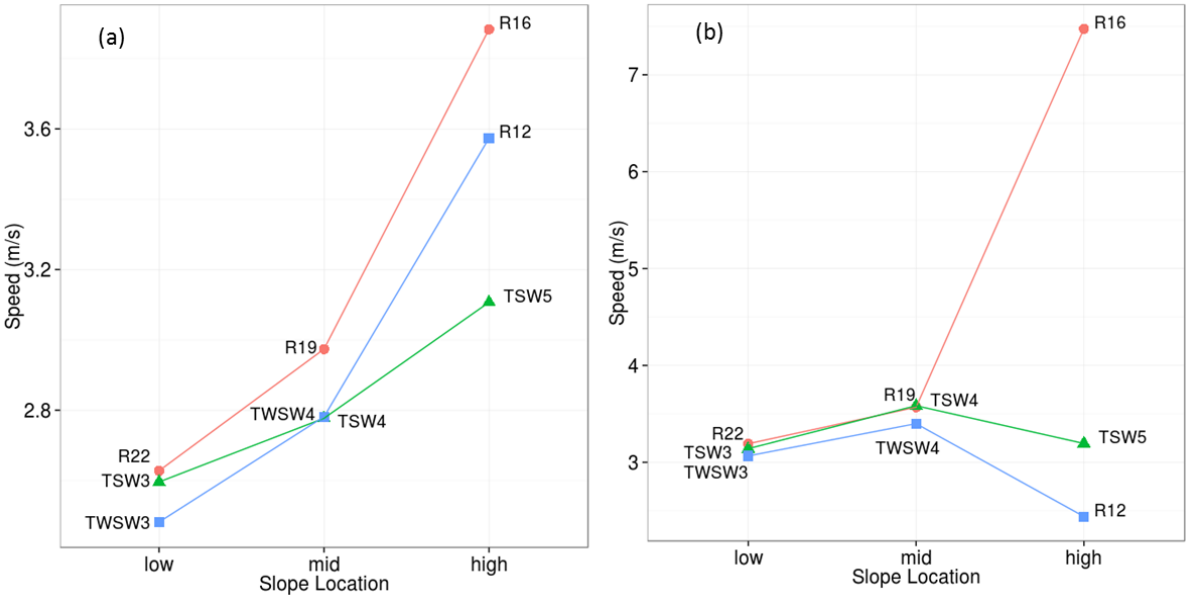


Fig. 5. Upslope (1100 local time) (a), afternoon (1600 local time) (b), and downslope (0000 local time) (c) flow regimes at Big Southern Butte during periods of weak synoptic flow between June-September 2010. Vectors are centered on sensor locations and represent the average hourly flow at a given sensor. Periods of strong synoptic forcing were removed prior to averaging.

812



813

814

815

816

817

818

Fig. 6. Average wind speeds for sensors at three slope locations (low, mid, and high) along three transects during the (a) upslope (1100 local time) and (b) downslope (0000 local time) flow regimes at Big Southern Butte.

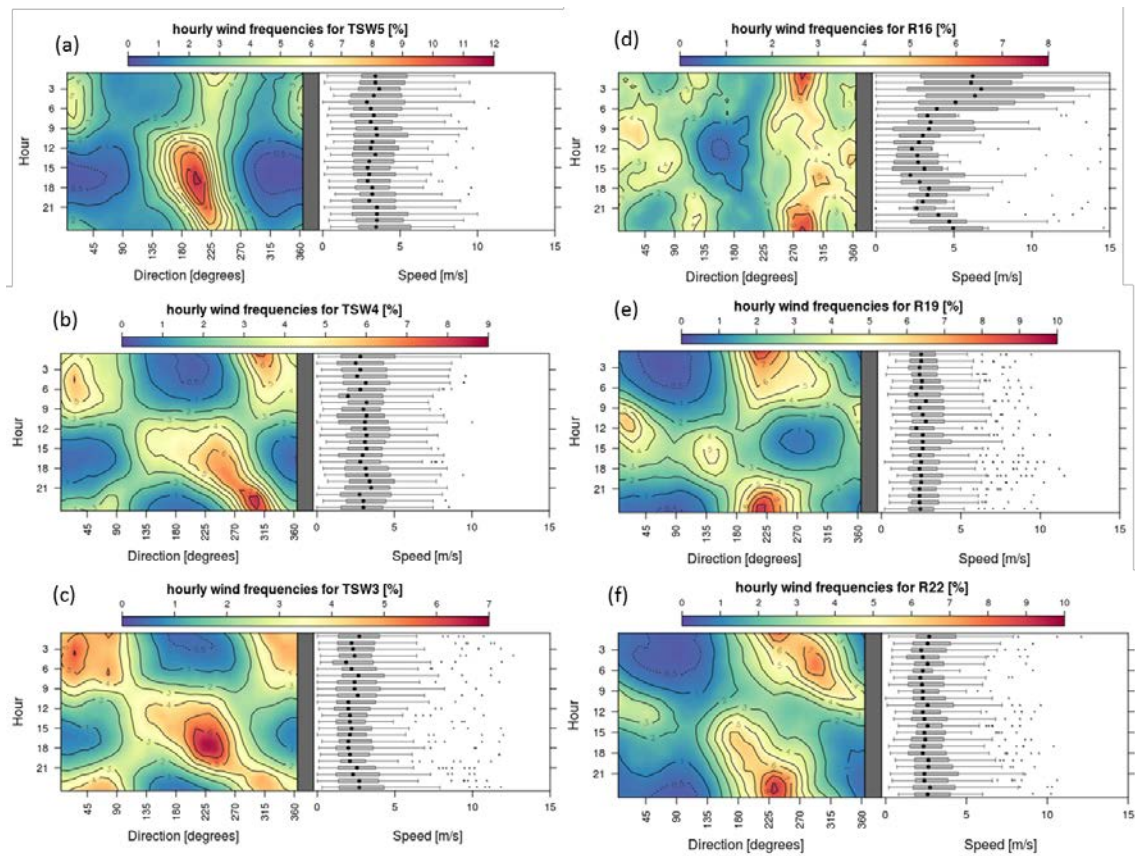


Fig.7. Contour plots of hourly wind frequencies and corresponding wind speeds for a transect on the southwest slope of Big Southern Butte (a)-TSW5 elevation 2067 m, (b)-TSW4 elevation 1750 m, (c)-TSW3 elevation 1630 m; and a transect on the northeast slope of Big Southern Butte (d)-R16 elevation 2080 m, (e)-R19 elevation 1720m, and (f)-R22 elevation 1550 m. Panels are ordered from higher elevation sensors (top panels) to lower elevation sensors (bottom panels). Periods of synoptic forcing were removed from this data.

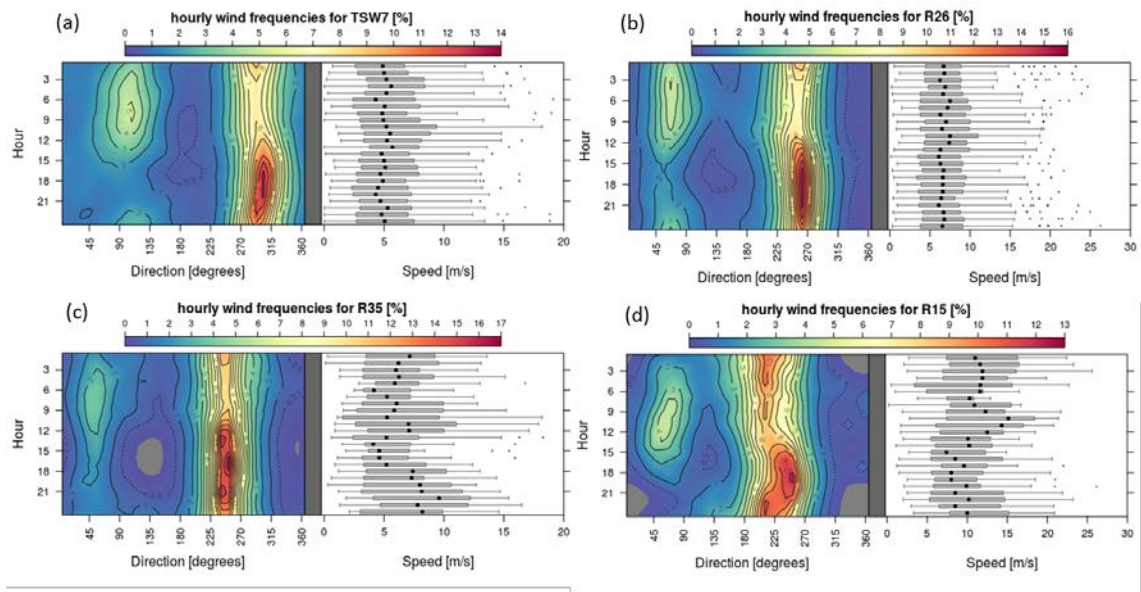


Fig. 8. Contour plots of hourly wind frequencies and corresponding wind speeds at four ridgetop locations at Big Southern Butte. (a)-TSW7 elevation 2217 m, (b)-R26 elevation 2100 m, (c)-R35 elevation 2200 m, (d)-R15 elevation 1980 m. Periods of strong synoptic forcing were removed from this data.

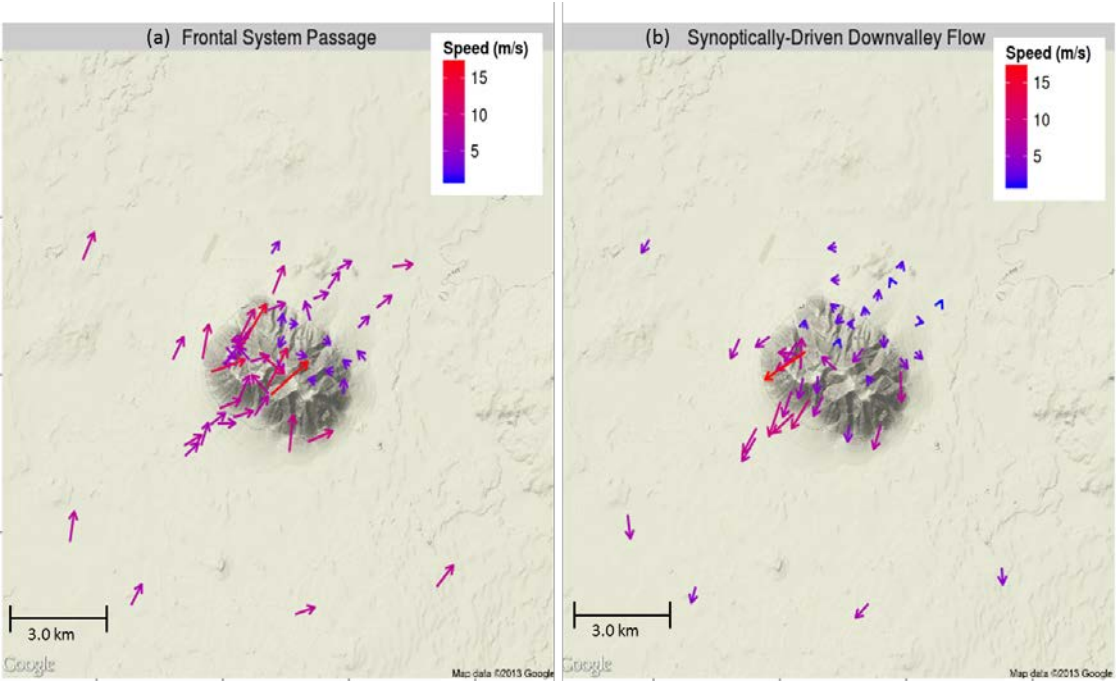


Fig. 9. Characteristic synoptically-driven regime events during the passage of a frontal system (1800 LT) (a) and during synoptically-enhanced downvalley flow on the Snake River Plain (2300 LT) (b) at Big Southern Butte during June-September 2010. Vectors represent the average hourly flow at a given sensor. Periods of weak synoptic forcing were removed prior to averaging.

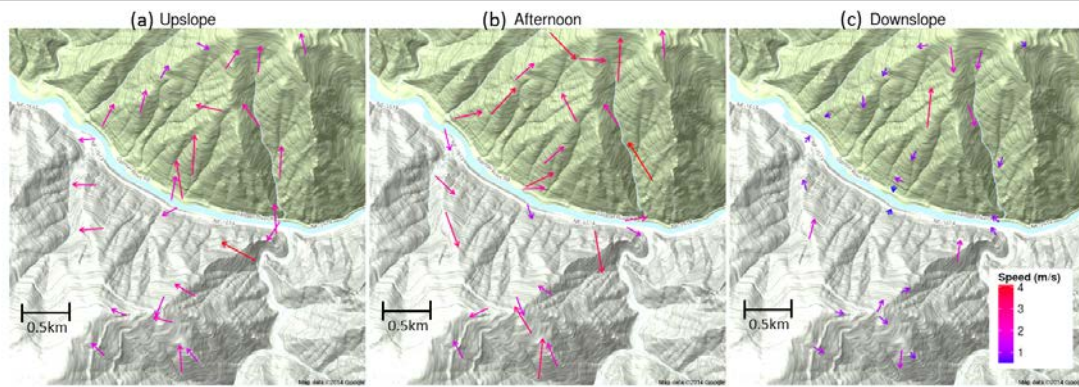


Fig. 10. Upslope (a) (1100 LT), afternoon (b) (1600 LT), and downslope (c) (0000 LT) regimes at the Salmon River Canyon site during periods of weak synoptic flow between July-September 2011. Vectors represent the average hourly flow at a given sensor. Periods of strong synoptic forcing were removed prior to averaging.

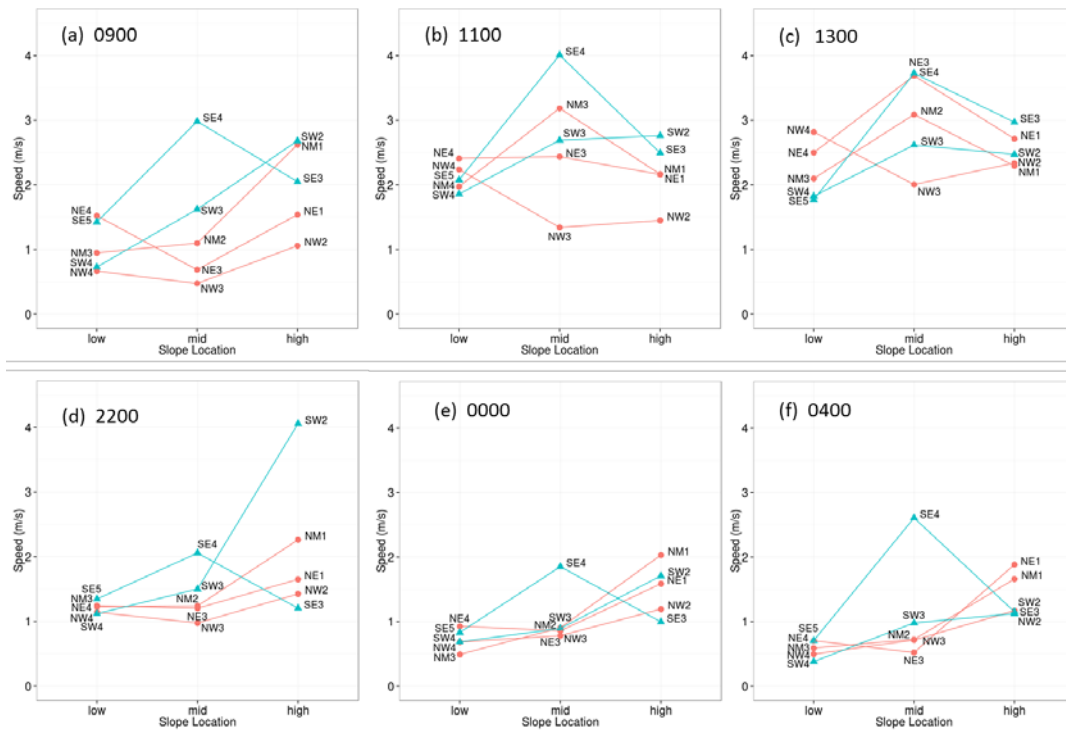


Fig. 11. Average wind speeds for sensors at three slope locations (low, mid, and high) along five transects during three hours of the upslope (a, b, c) and downslope (d, e, f) flow regimes at the Salmon River Canyon site. Blue and red lines are transects on the south and north side of the river, respectively.

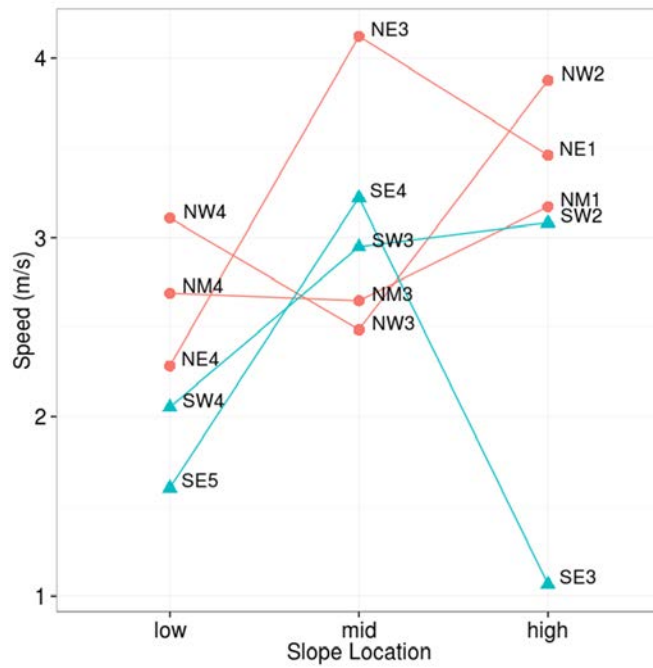


Fig. 12. Average wind speeds for sensors at three slope locations (low, mid, and high) along five transects during the afternoon flow regime (1700) at the Salmon River Canyon site. Blue and red lines are transects on the south and north side of the river, respectively.

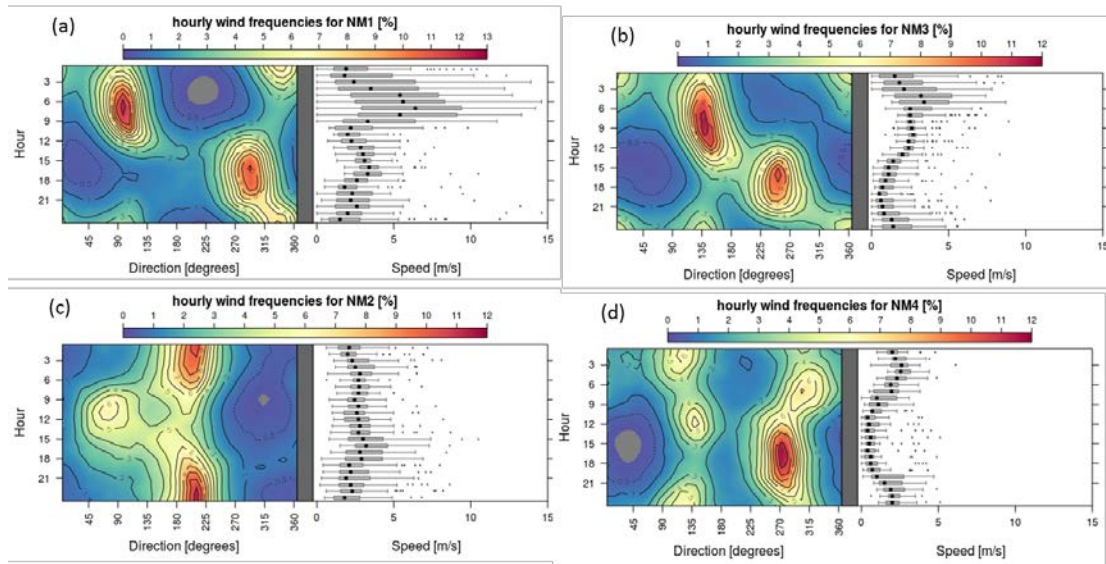


Fig. 13. Contour plots of hourly wind frequencies and corresponding wind speeds for the NM transect at the Salmon River Canyon site. (a)-NM1 is near the ridgetop at 1734 m. (b)-NM2 is at 1210 m. (c)-NM3 is at 1080 m. (d)-NM4 is at 540 m and is near the canyon bottom. All data were used.

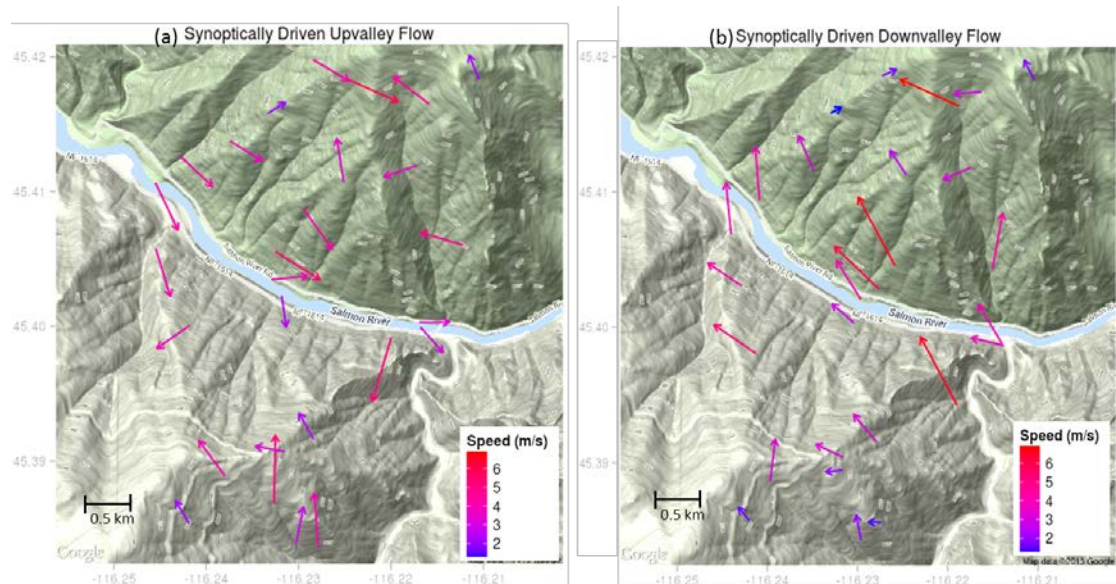


Fig. 14. Characteristic synoptically driven upvalley flow (1500 LT) (a) and downvalley flow (1100 LT) (b) at the Salmon River Canyon site during July-September 2011. Vectors represent the average hourly flow at a given sensor. Periods of weak synoptic forcing were removed prior to averaging.

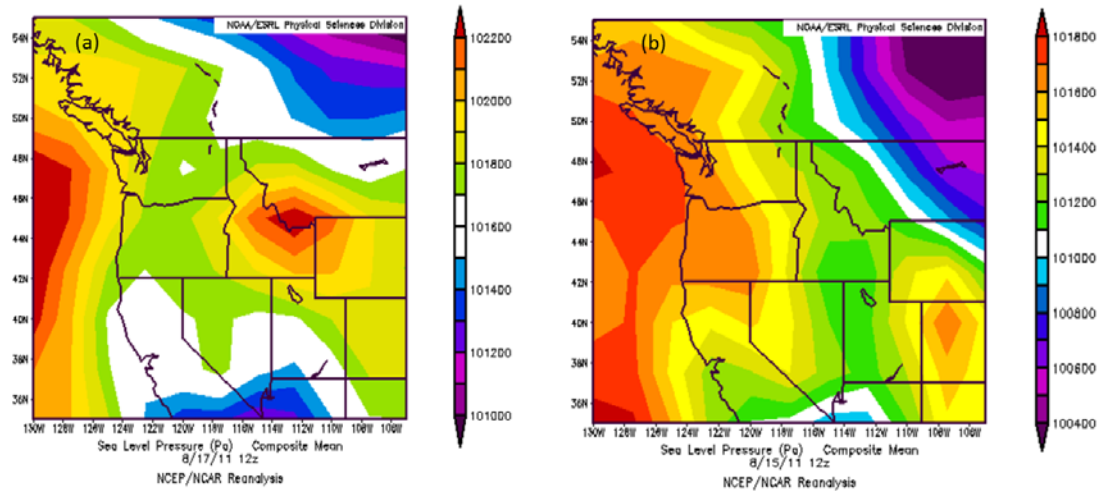


Fig. 15. Synoptic-scale surface pressure conditions conducive to enhanced easterly flow (a) and typical diurnal flow scenarios (b) at the Salmon River Canyon site (North American Regional Reanalysis data courtesy of National Center for Environmental Prediction).

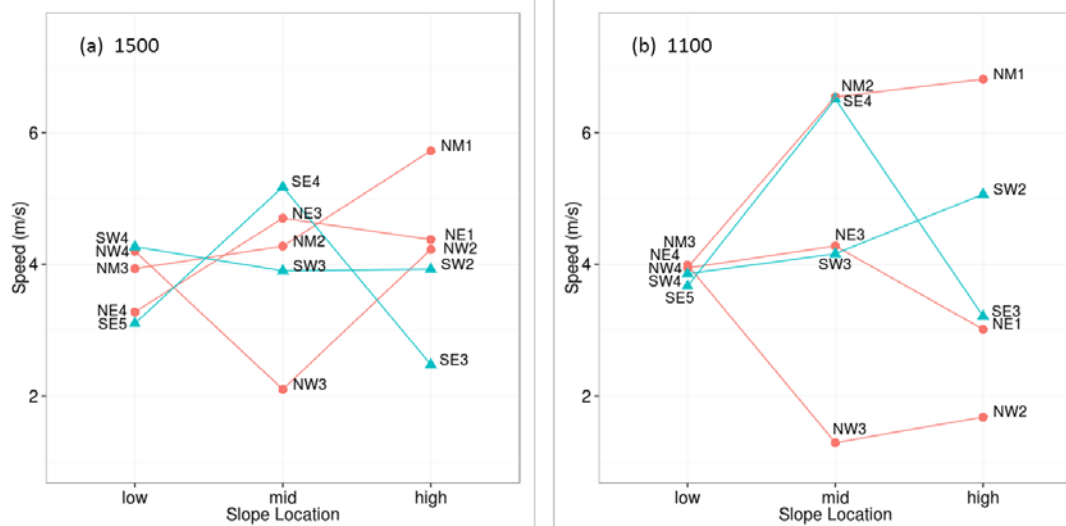


Fig. 16. Average wind speeds for sensors at three slope locations (low, mid, and high) along five transects during the synoptically driven upvalley (a) and synoptically driven downvalley (b) flow regimes at the Salmon River Canyon site. Blue and red lines are transects on the south and north side of the river, respectively.

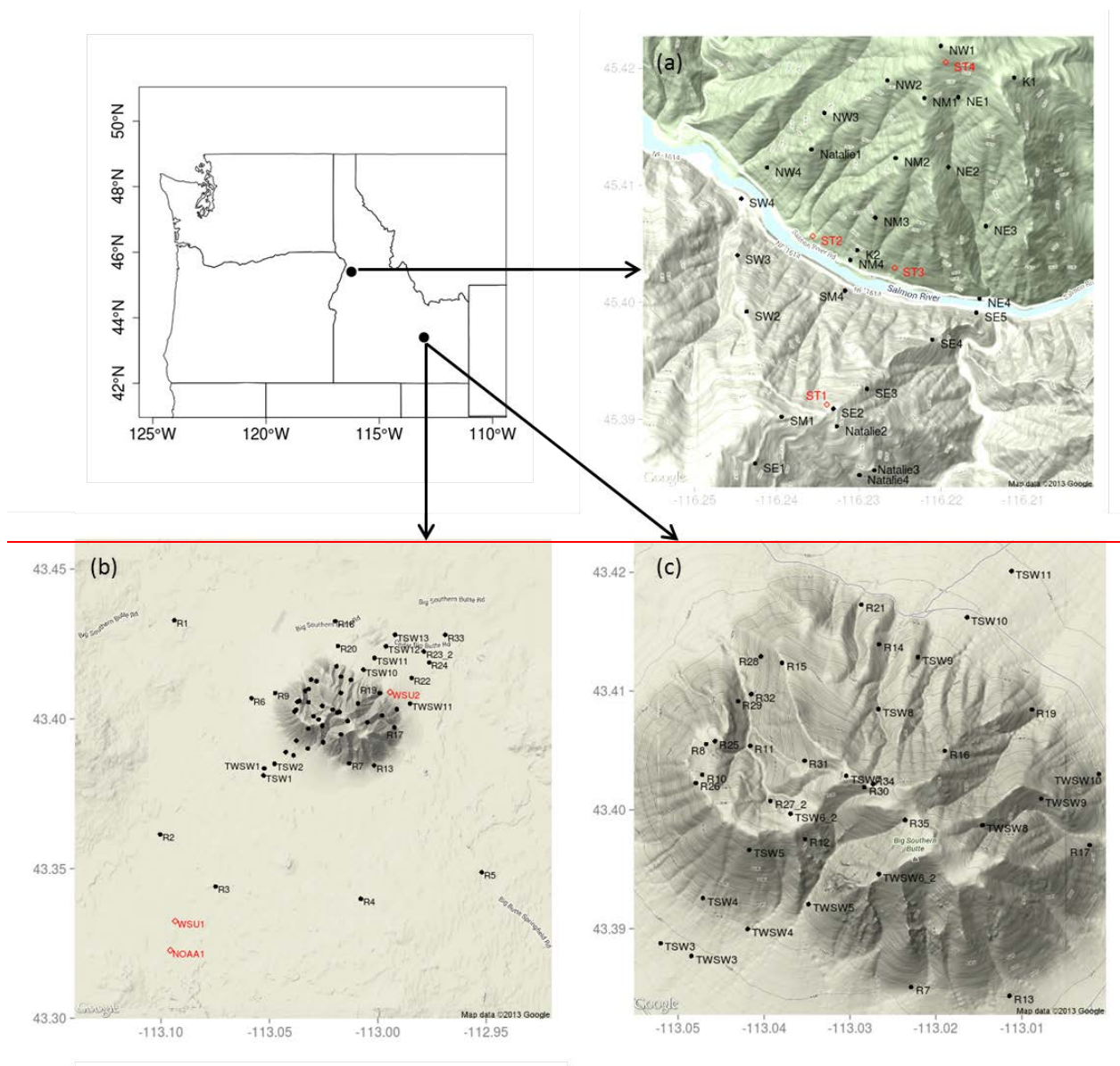


Fig. 1. Site overview and sensor layouts at the Salmon River Canyon (a) and Big Southern Butte (b, c). Black circles indicate surface sensors. Red diamonds indicate sonic-anemometers and vertical profiling sensors.



Fig. 2. Snake River Plain and prominent drainages surrounding the BSB study site.

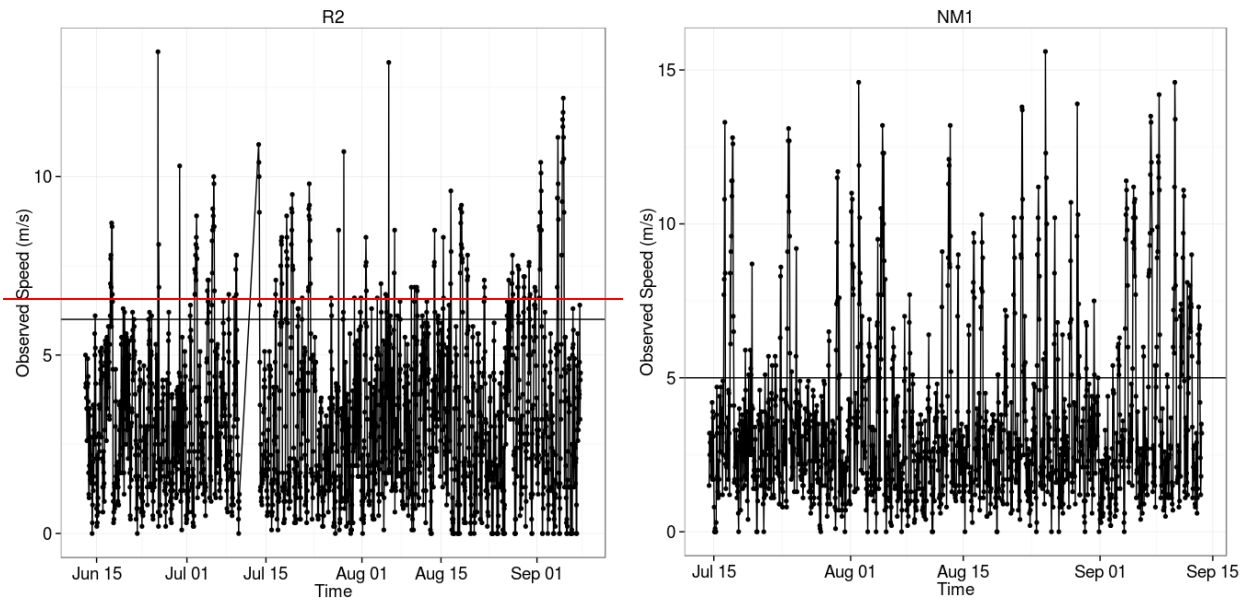


Fig. 3. Observed hourly wind speeds for R2 at BSB and NM1 at SRC. The horizontal line indicates the threshold speed chosen to partition synoptically driven events from diurnal events.

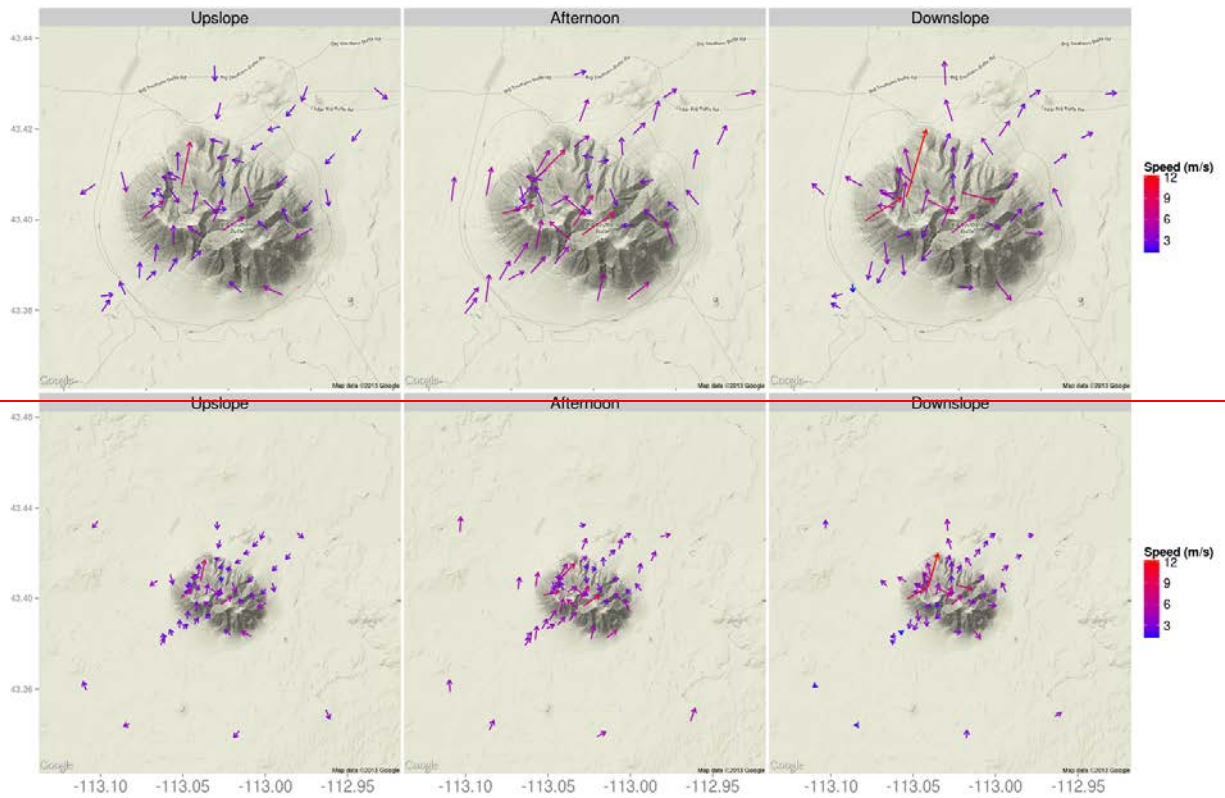


Fig. 4. Upslope (1100 LT), afternoon (1600 LT), and downslope (0000 LT) flow regimes at BSB during periods of weak synoptic flow between June-September 2010. Vectors represent the average hourly flow at a given sensor. Vectors are centered on sensor locations. Periods of strong synoptic forcing were removed prior to averaging. Upper strip is zoomed in on the butte. Lower strip is zoomed out to show entire study area.

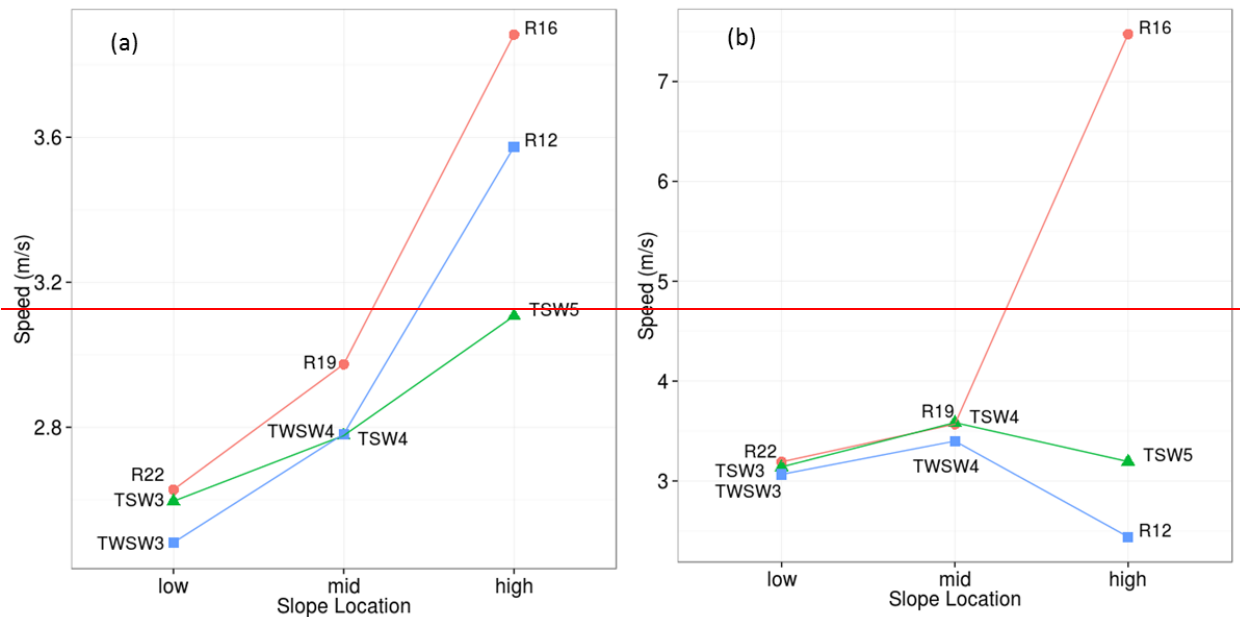


Fig. 5. Average wind speeds for sensors at three slope locations (low, mid, and high) along three transects during the (a) upslope (1100 LT) and (b) downslope (0000 LT) flow regimes at BSB.

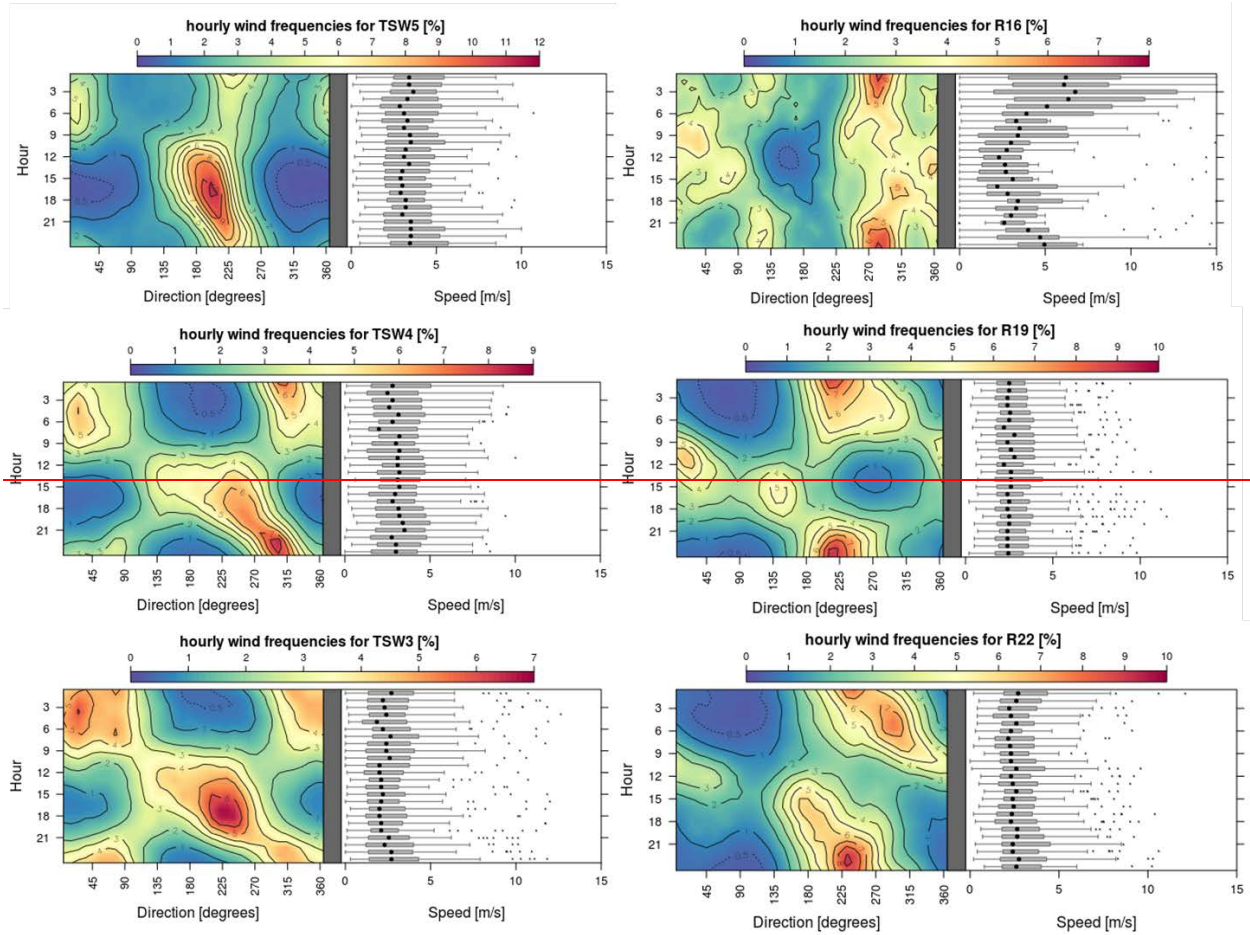


Fig. 6. Contour plots of hourly wind frequencies and corresponding wind speeds for a transect on the southwest slope of Big Southern Butte (left panels) and a transect on the northeast slope of Big Southern Butte (right panels). Panels are ordered from higher elevation sensors (top panels) to lower elevation sensors (bottom panels). Periods of synoptic forcing were removed from this data.

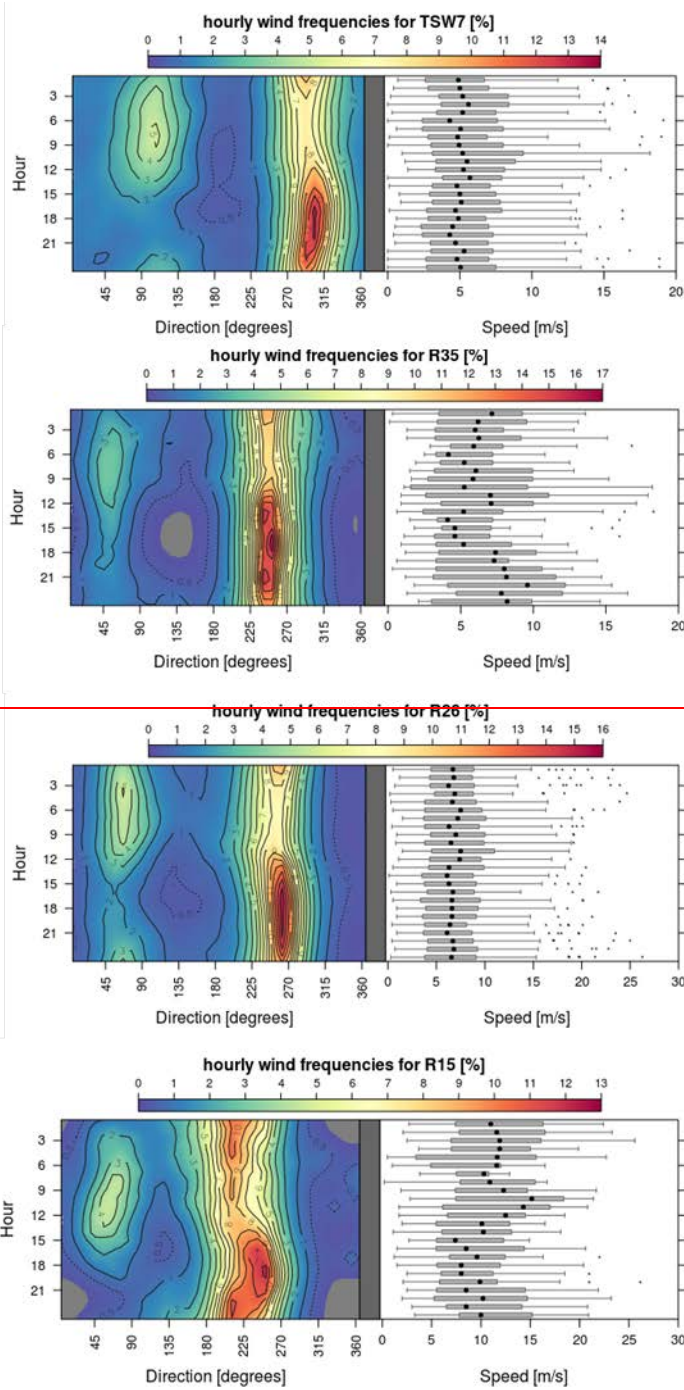


Fig. 7. Contour plots of hourly wind frequencies and corresponding wind speeds for four ridgetop locations at Big Southern Butte. Periods of strong synoptic forcing were removed from this data.

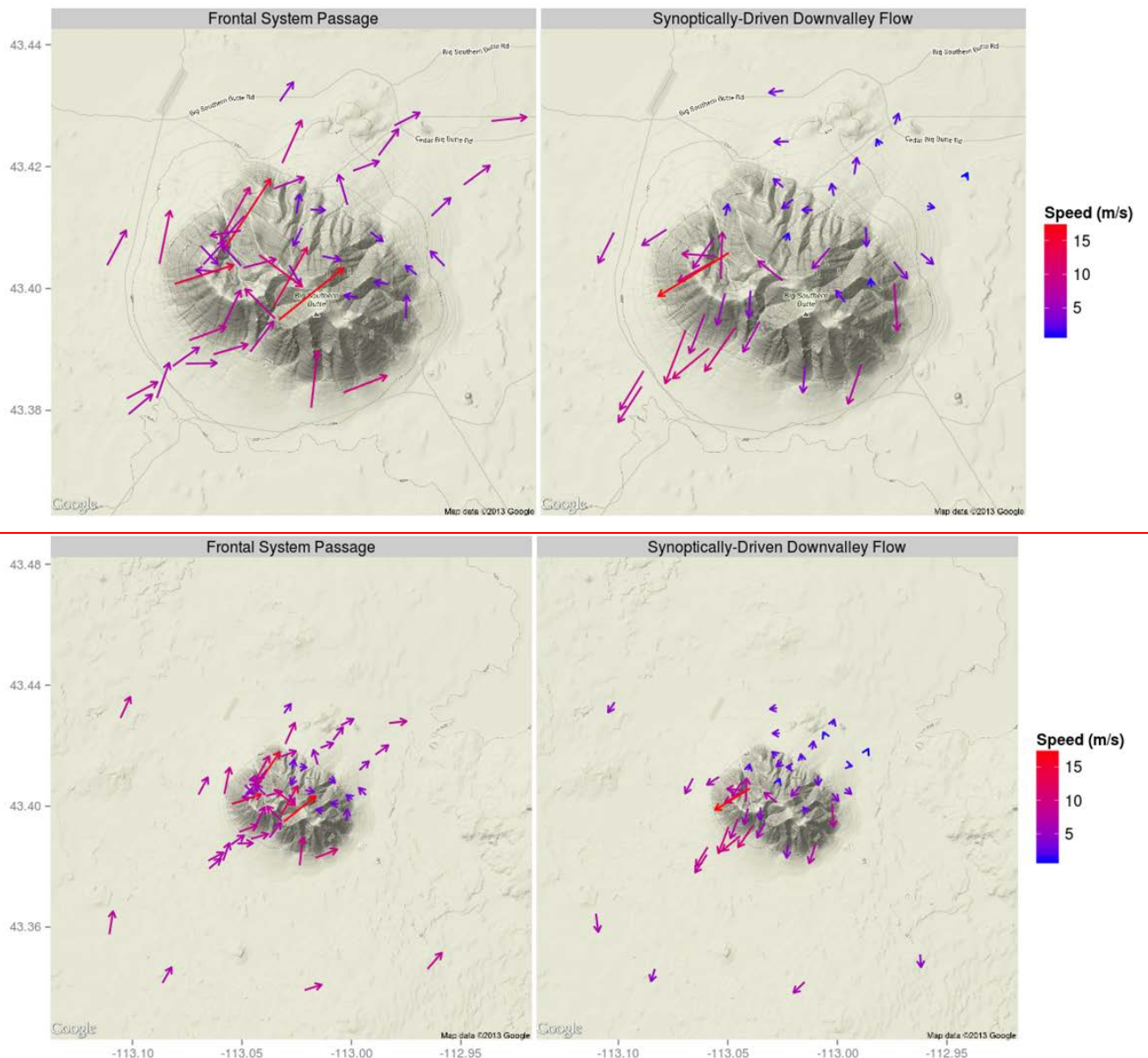


Fig. 8. Characteristic synoptically-driven regime events during the passage of a frontal system (1800 LT) and during synoptically-enhanced downvalley flow on the Snake River Plain (2300 LT) at BSB during June-September 2010. Vectors represent the average hourly flow at a given sensor. Periods of weak synoptic forcing were removed prior to averaging. Lower strip is zoomed out to show entire study area.

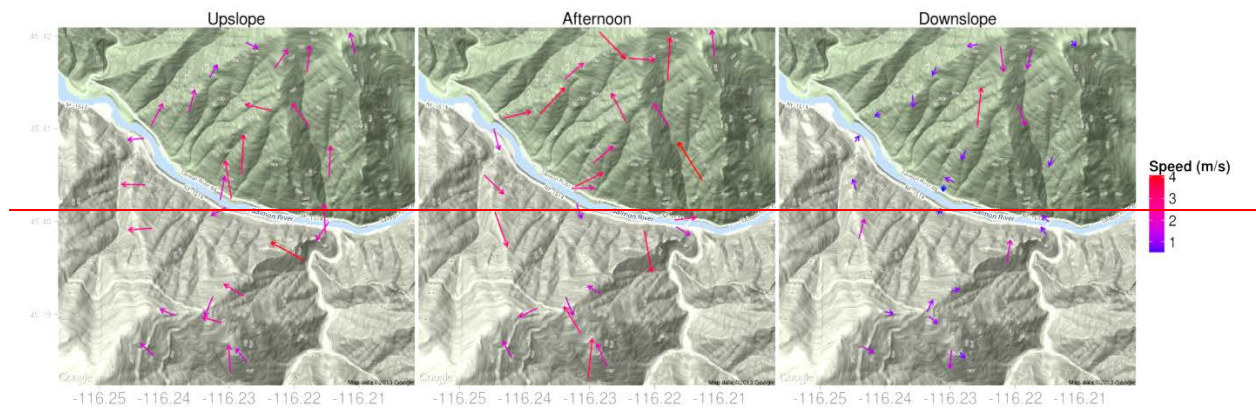


Fig. 9. Upslope (1100 LT), afternoon (1600 LT), and downslope (0000 LT) regimes at SRC during periods of weak synoptic flow between July-September 2011. Vectors represent the average hourly flow at a given sensor. Periods of strong synoptic forcing were removed prior to averaging.

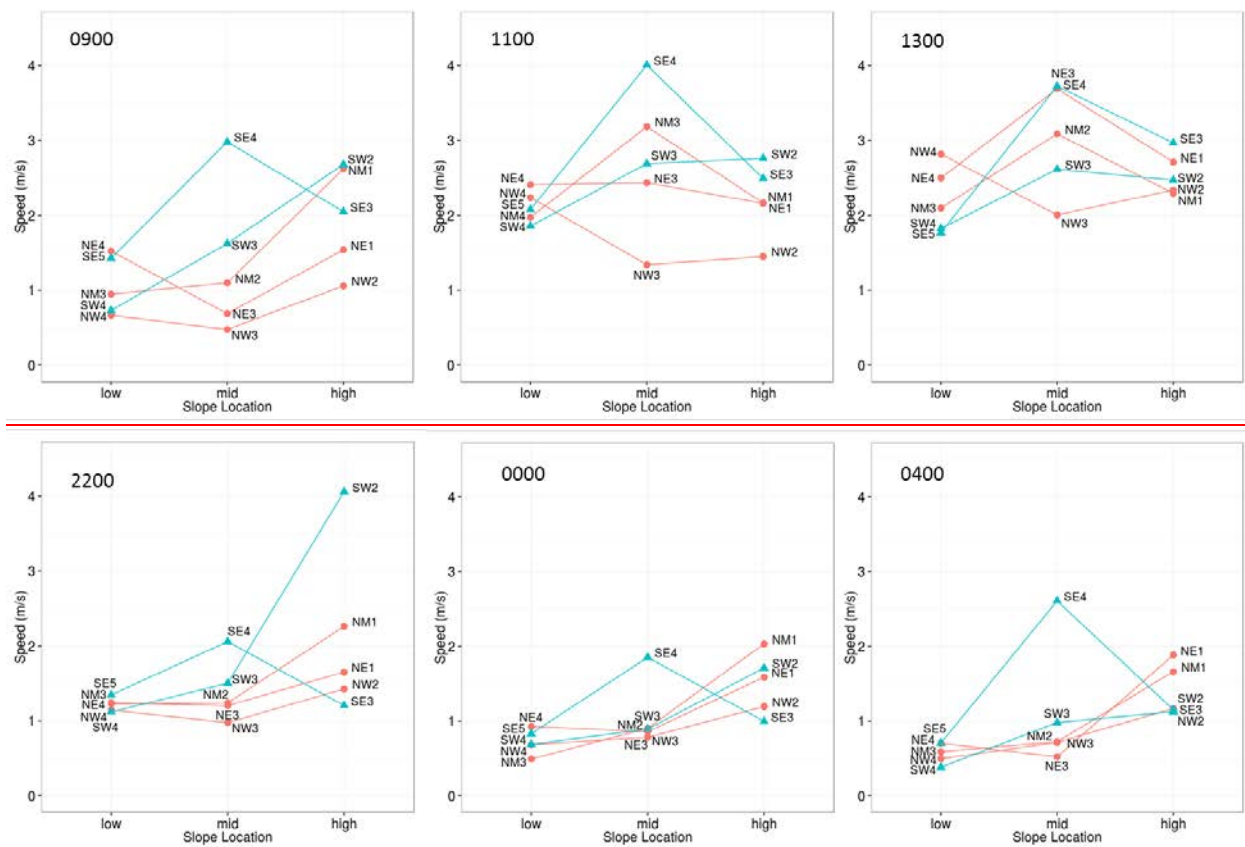


Fig. 10. Average wind speeds for sensors at three slope locations (low, mid, and high) along five transects during three hours of the upslope (top panels) and downslope (bottom panels) flow regimes at SRC. Blue and red lines are transects on the south and north side of the river, respectively.

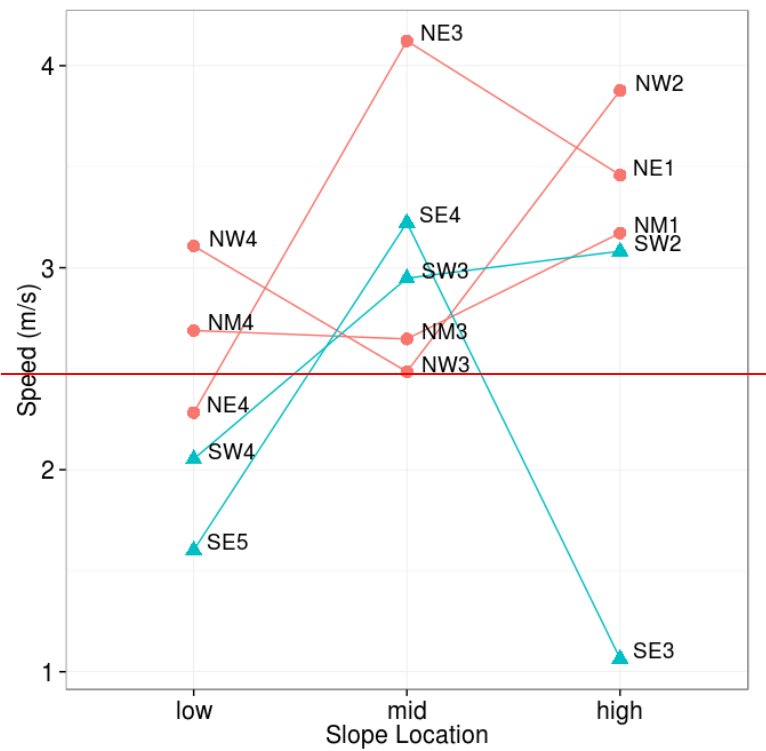


Fig. 11. Average wind speeds for sensors at three slope locations (low, mid, and high) along five transects during the afternoon flow regime (1700) at SRC. Blue and red lines are transects on the south and north side of the river, respectively.

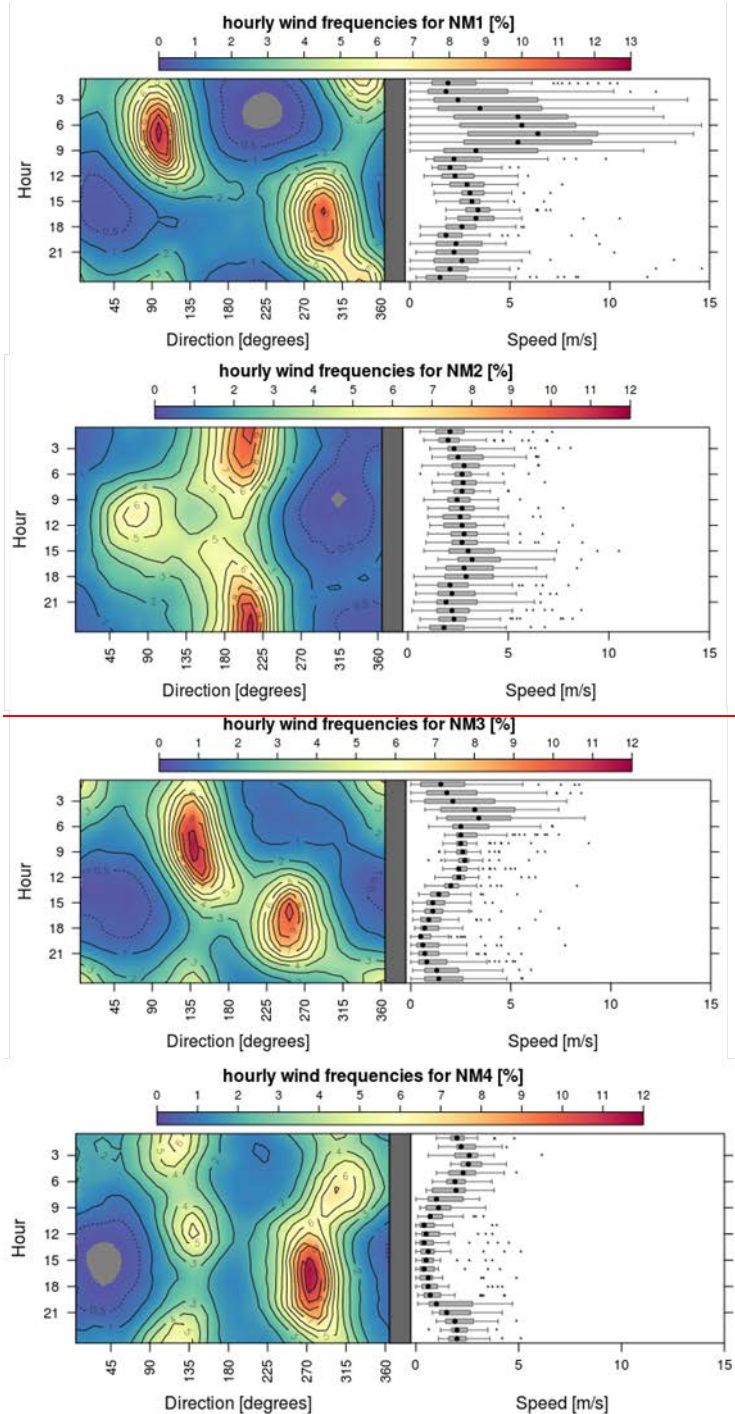


Fig. 12. Contour plots of hourly wind frequencies and corresponding wind speeds for the NM transect at SRC. NM1 is near the ridgetop. NM4 is near the canyon bottom. All data were used.

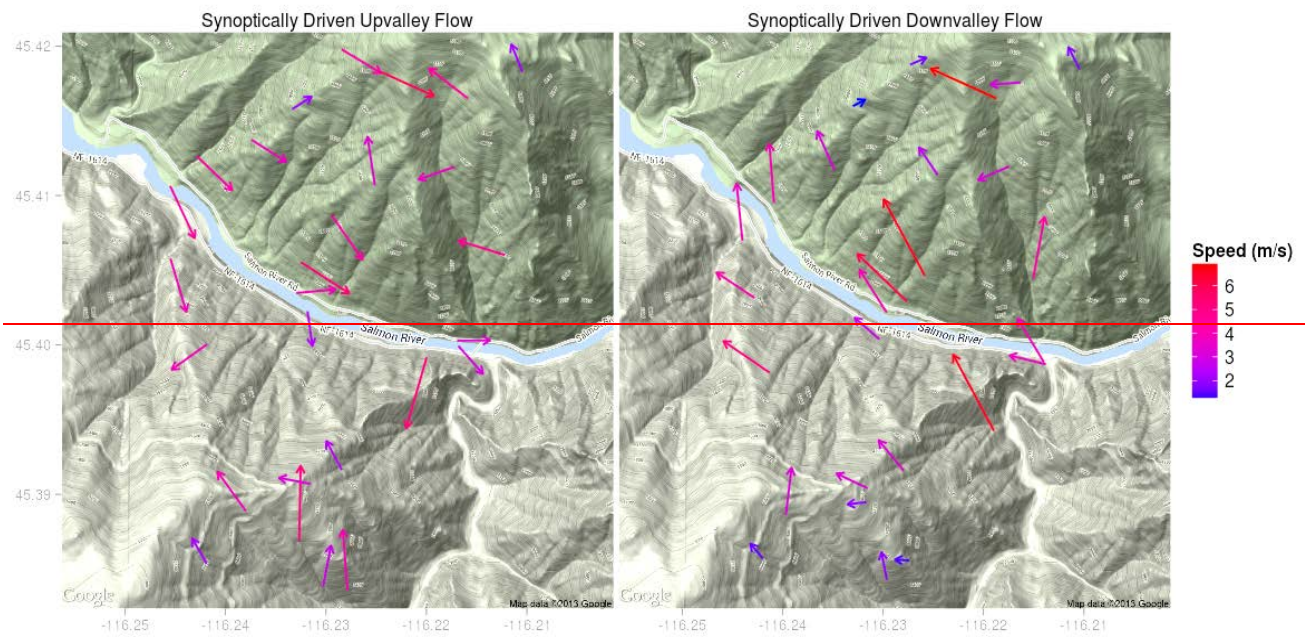


Fig. 13. Characteristic synoptically driven upvalley flow (1500 LT) and downvalley flow (1100 LT) at SRC during July-September 2011. Vectors represent the average hourly flow at a given sensor. Periods of weak synoptic forcing were removed prior to averaging.

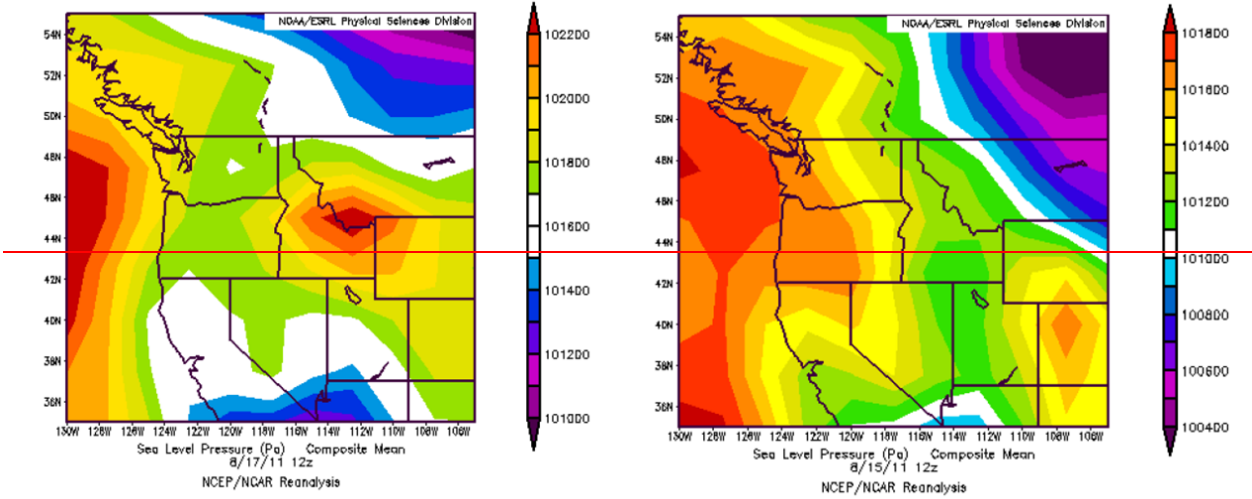


Fig. 14. Synoptic-scale surface pressure conditions conducive to enhanced easterly flow (left) and typical diurnal flow scenarios (right) at SRC (North American Regional Reanalysis data courtesy of National Center for Environmental Prediction).

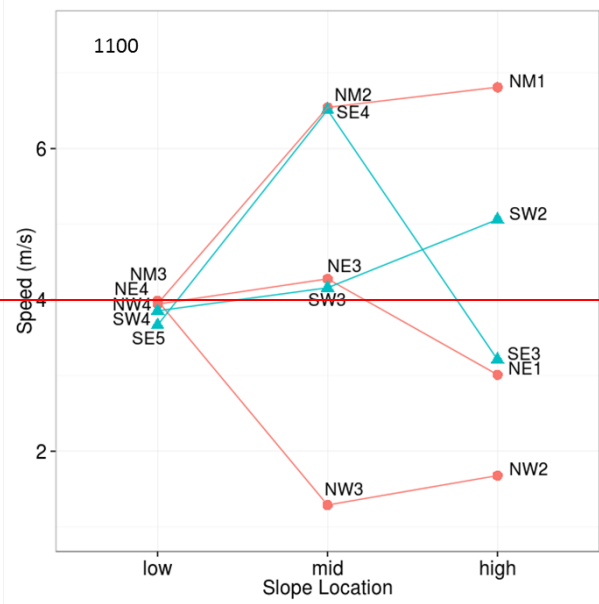
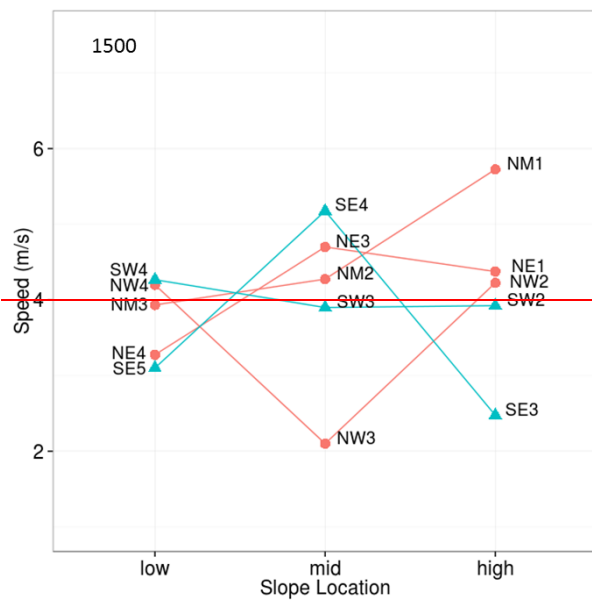


Fig. 15. Average wind speeds for sensors at three slope locations (low, mid, and high) along five transects during the synoptically driven upvalley (left) and synoptically driven downvalley (right) flow regimes at SRC. Blue and red lines are transects on the south and north side of the river, respectively.